Boris I. Prilutsky
Donald H. Edwards *Editors*

Neuromechanical Modeling of Posture and Locomotion

Springer

Editors
Boris I. Prilutsky
Georgia Institute of Technology
Atlanta
Georgia
USA

Donald H. Edwards
Georgia State University
Atlanta
Georgia
USA

Printed on acid-free paper

Chapter 5
Modeling the Organization of Spinal Cord Neural Circuits Controlling Two-Joint Muscles

Natalia A. Shevtsova, Khaldoun Hamade, Samit Chakrabarty, Sergey N. Markin, Boris I. Prilutsky and Ilya A. Rybak

Abstract The activity of most motoneurons controlling one-joint muscles during locomotion are locked to either extensor or flexor phase of locomotion. In contrast, bifunctional motoneurons, controlling two-joint muscles such as posterior biceps femoris and semitendinosus (PBSt) or rectus femoris (RF), express a variety of activity patterns including firing bursts during both locomotor phases, which may depend on locomotor conditions. Although afferent feedback and supraspinal inputs significantly contribute to shaping the activity of PBSt and RF motoneurons during real locomotion, these motoneurons show complex firing patterns and variable behaviors under the conditions of fictive locomotion in the immobilized decerebrate cat, i.e., with a lack of patterned supraspinal and afferent inputs. This suggests that firing patterns of PBSt and RF motoneurons are defined by neural interactions inherent to the locomotor central pattern generator (CPG) within the spinal cord. In this study, we use computational modeling to suggest the architecture of spinal circuits representing the locomotor CPG and the connectivity pattern of spinal interneurons defining the behavior of bifunctional PBSt and RF motoneurons. The proposed model reproduces the complex firing patterns of these motoneurons during

N. A. Shevtsova (✉) · K. Hamade · S. N. Markin · I. A. Rybak
Department of Neurobiology and Anatomy, Drexel University College of Medicine,
2900 W. Queen Lane, Philadelphia, PA 19129, USA
e-mail: Natalia.Shevtsova@drexelmed.edu

K. Hamade
e-mail: Khaldoun.Hamade@drexelmed.edu

S. N. Markin
e-mail: smarkin@drexelmed.edu

S. Chakrabarty
School of Biomedical Sciences, Faculty of Biology, University of Leeds,
Garstang Building, Leeds, West Yorkshire LS2 9JT, UK
e-mail: s.chakrabarty@leeds.ac.uk

B. I. Prilutsky
School of Applied Physiology, Center for Human Movement Studies, Georgia Institute
of Technology, 555 14th Street NW, Atlanta, GA 30332, USA

fictive locomotion under different conditions including spontaneous deletions of flexor and extensor activities and provides insights into the organization of spinal circuits controlling locomotion in mammals.

Keywords Spinal cord · Two-joint muscles · Fictive locomotion · Central pattern generator · Computational modeling

Abbreviations

CPG	Central pattern generator
EMG	Electromyoagam
ENG	Electroneurogram
GS	Gastrocnemius combined with soleus
LGS	Lateral gastrocnemius combined with soleus
MG	Medial gastrocnemius
MLR	Mesencephalic locomotor region
PB	Posterior biceps femoris
PBSt	PB combined with semitendinosus
PF	Pattern formation
Plant	Plantaris
RF	Rectus femoris
RG	Rhythm generator
Sart	Sartorius
SmAB	Semimembranosus combined with anterior biceps femoris
St	Semitendinosus
TA	Tibialis anterior
UBG	Unit burst generator

5.1   Introduction

The bipartite half-center organization of the spinal locomotor central pattern generator (CPG) was originally proposed by T. Graham Brown (1914) and then expanded by Lundberg, Jankowska and their colleagues (e.g., Jankowska et al. 1967a, b; Lundberg 1981). According to this concept, the locomotor rhythmic activity is generated by the alternating activity of two populations of excitatory interneurons (the "half-centers") mutually inhibiting each other via inhibitory interneurons. This alternating half-center activity directly controls alternating activation of extensor and flexor motoneurons whose activity is locked to one of the two locomotor phases. However, the activity of motoneuron pools controlling the muscles spanning more than one joint (e.g., the two-joint muscles) is more complicated and often depends on locomotor conditions. In particular, motoneuron pools controlling such muscles as posterior biceps femoris and semitendinosus (PB and St or PBSt, hip extensor and knee flexor) and rectus femoris (RF, hip flexor and knee extensor) express a variety of activity patterns depending on gait, speed, and slope of locomotion, and/or other

locomotor conditions (Halbertsma 1983; Pratt et al. 1996; Carlson-Kuhta et al. 1998; Smith et al. 1998a). The activity of PBSt during real locomotion can be characterized as flexor- or extensor-related, depending on the primary muscle group with which it is co-active, or as biphasic (Grillner 1981; Halbertsma 1983; Smith et al. 1998b). RF also shows similar variability in activity patterns during locomotion that also depends on gait and locomotor conditions (Pratt et al. 1996; Smith et al. 1998b).

The complex activity patterns generated by motoneurons controlling two-joint muscles have been considered as a strong argument against a half-center (bipartite) organization of the CPG (discussed by Grillner 1981; Stein and Smith 1997). In contrast, Perret and colleagues (Perret 1983; Orsal et al. 1986; Perret et al. 1988) suggested that the PBSt and RF motoneuron pools may receive excitatory and inhibitory inputs from both flexor and extensor CPG half-centers and proposed several schematics of spinal circuits that could potentially generate the complex PBSt and RF patterns within a framework of the bipartite locomotor CPG organization. The principal point of the proposed architecture was the existence of additional interneurons interposed between the rhythm generator and PBSt and RF motoneurons that could provide shaping of their firing patterns under control of supraspinal and/or afferent signals (Perret 1983). In this architecture (see Fig. 5.1), intermediate neuron populations are controlled by excitatory inputs from the CPG and afferent pathways and shape PBSt and RF activities through excitatory and inhibitory influences.

However, although afferent feedback and supraspinal inputs may significantly contribute to shaping activity of PBSt and RF motoneurons during real locomotion, these motoneurons express a wide repertoire of firing patterns during fictive locomotion in decerebrate immobilized cats in the absence of sensory feedback and patterned supraspinal inputs (Grillner and Zangger 1979; Perret and Cabelguen 1980; Perret 1983; Orsal et al. 1986; Guertin et al. 1995; Markin et al. 2012). Moreover, with afferent stimulation, the spontaneous activity of PBSt and RF motoneurons was reportedly altered from being flexor-related to extensor-related (Perret 1983) or biphasic (McCrea and Chakrabarty 2007; Shevtsova et al. 2007; Hamade et al. 2008). Such a wide repertoire of PBSt and RF motoneuron firing behaviors during fictive locomotion have never been explained or reproduced with computational models.

Rybak et al. (Rybak et al. 2006a, b; McCrea and Rybak 2007, 2008) have recently proposed a two-level organization of the locomotor CPG in which a bipartite rhythm generator (RG) controls a specially organized pattern formation (PF) network that in turn projects to motoneurons and controls their behavior (Fig. 5.2). The two-level CPG architecture permits separate control of the locomotor rhythm and motoneuron activity. The first level, RG, defines the locomotor rhythm and the durations of the flexor and extensor phases, and the second level, the PF network, transforms the RG activity to activity patterns of different motoneuron pools. The two-level CPG model was able to reproduce multiple effects of afferent stimulation during fictive locomotion as well as the specific behavior of flexor and extensor motoneurons during spontaneous deletions (missing bursts) of motoneuron activity (Rybak et al. 2006a, b; McCrea and Rybak 2007, 2008; Shevtsova 2015). However, this model included only two antagonist motoneuron pools (flexor and extensor, see Fig. 5.2) and the generation of more complex activity patterns, such as patterns of PBSt and RF, was not considered.
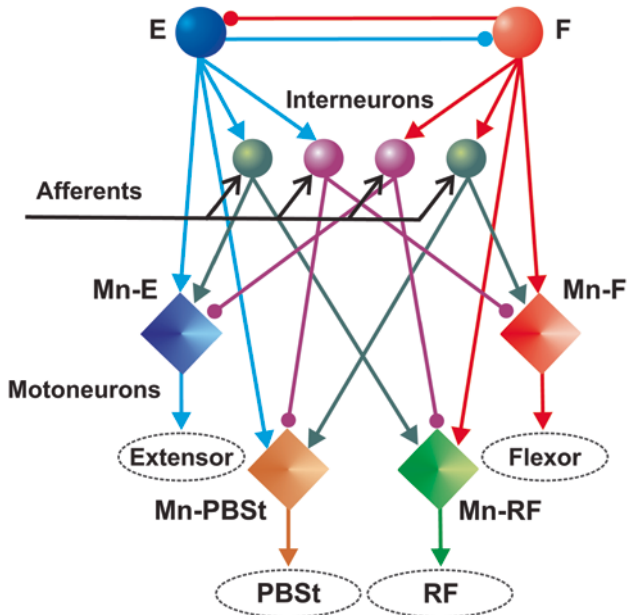
Fig. 5.1 Hypothetical network capable of generating the PBSt and RF activity patterns. The central rhythm generator (*F—E*) provides the alternating flexor-extensor activity. The flexor half-center, *F*, directly excites the flexor and RF motoneuron pools while the extensor half-center, *E*, directly excites the extensor and PBSt motoneurons. Additional interneuron populations of alternative reflex pathways are influenced by afferent inputs and provide complimentary excitatory/inhibitory signals to motoneuron populations. In this and following figures, populations of interneurons are represented by *spheres*; excitatory and inhibitory synaptic connections are indicated by lines ended with arrows and small circles, respectively; populations of motoneurons are represented by diamonds. Modified from (Perret 1983)

Here we propose a possible organization of spinal circuits in the frameworks of a two-level CPG organization allowing the model to generate different patterns of motoneuron activity including the complex patterns of the PBSt and RF observed during fictive locomotion, as well as to reproduce the variety of changes of these patterns during deletions.

5.2 Patterns of PBSt and RF Activity During fictive Locomotion

5.2.1 Data

Experimental data used in this study represent series of recordings of activity of different spinal nerves from decerebrate immobilized cat preparations during fictive locomotion induced by electrical stimulation of the brainstem mesencephalic
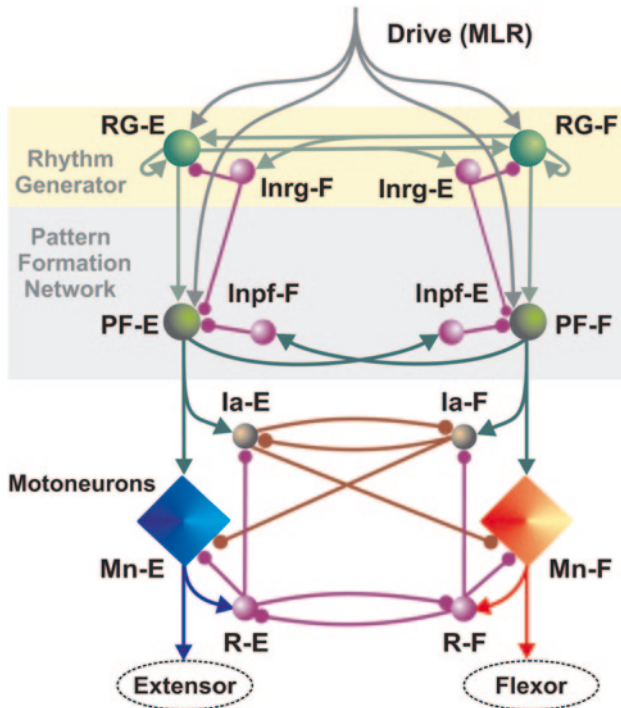
Fig. 5.2 Schematic of the two-level locomotor CPG model by (Rybak et al. 2006a). Note that for consistency with the current model description we slightly changed the names of the inhibitory interneuron populations Inrg-E, Inrg-F, Inpf-E and Inpf-F from those in the basic model given in (Rybak et al. 2006a, b). The extension E or F in a population name corresponds now to the phase in which this population is active. Modified from (Rybak et al. 2006a)

locomotor region (MLR). These data were collected for many years in the laboratories of Drs. McCrea and Jordan at the Spinal Cord Research Centre, University of Manitoba, Winnipeg, Canada. All experiments were performed in compliance with the guidelines set out by the Canadian Council on Animal Care and the University of Manitoba. No new animal experiments were performed for the present study.

Motoneuron activity during fictive locomotion was recorded extracellularly as electroneurograms (ENGs) from multiple hindlimb nerves. Nerve recordings were rectified and low-pass filtered before digitization (for details see Guertin et al. 1995; Lafreniere-Roula and McCrea 2005). Data were analyzed from experiments which included records from RF nerve as well as PB or St nerves or the combined PB and St (PBSt) nerves. As described above, the locomotor activities of two-joint muscles can vary widely depending upon behavioral or experimental conditions. However, the particular pattern of motoneuron activity of PBSt or RF occurring in a given fictive locomotion preparation generally remained unchanged during the course of an experiment despite changes in locomotor period or variations in MLR stimulus intensity employed during the experiment. When recorded separately during fictive locomotion, the ENGs from PB and St (both muscles are hip extensors and

knee flexors) exhibited similar firing pattern regardless of whether their activity was flexor-phase or extensor-phase related. This similarity justified the common practice of using recordings from the combined PBSt nerves.

## 5.2.2 Classification of PBSt and RF Firing Patterns During Fictive Locomotion

The typical patterns of activity of PBSt and RF during fictive locomotion are shown in Fig. 5.3. Our previous analysis (Markin et al. 2012) described three distinct patterns of PBSt motoneuron activity and two patterns of RF motoneuron activity occurring during fictive locomotion (Fig. 5.4, panels b and c, respectively). In Fig. 5.4, the typical patterns of flexor (Sart) and extensor (SmAB) activity are also shown for reference. This figure shows that during fictive locomotion, PBSt usually exhibits one of the following three ENG activity patterns: (1) a single burst at the beginning of the flexor phase (*type 1*, observed in 73 % of PBSt records, Fig. 5.4b, upper trace; see examples in Fig. 5.3a1, a2, d1, d2) that is usually short in duration (less than 30 % of the flexor phase, *type 1a,* Fig. 5.3a1, d1, d2) but sometimes longer (up to 70 % of the flexor phase, *type 1b*, Fig. 5.3a2); (2) a typical extensor activity, i.e., firing throughout the entire extensor phase (*type 2*, 9 % of cases, Fig. 5.4b, middle trace; see example in Fig. 5.3b); and (3) a biphasic pattern, consisting of a short first burst at the beginning of the flexor phase and a longer second burst throughout the extensor phase (*type 3*, 18 % of cases, Fig. 5.4b, bottom trace, examples are in Fig. 5.3c1, c2).

RF usually exhibited one of the following two ENG patterns: (1) a single burst at the end of the flexor phase (*type 1*, observed in 53 % of RF records, Fig. 5.4c, upper trace, example is shown in Fig. 5.3b, d1) or (2) a biphasic pattern consisting of a burst at the end of the flexor phase and an additional burst at the end of the extensor phase (*type 2*, 47 % of cases, Fig. 5.4c, bottom trace, see example in Fig. 5.3d2). In all experiments with simultaneous recordings, PBSt and RF never were active simultaneously (see for example, see Fig. 5.3b, d1, d2). Possible combinations of PBSt and RF ENG activities recorded simultaneously in fictive locomotion experiments are shown in Fig. 5.4d1–d4.

5.2.3 Activity of PBSt and RF Motoneurons During Spontaneous Deletions

Deletions represent brief periods of inactivity (missing one or several consecutive bursts) occurring spontaneously during generation of locomotor activity simultaneously in multiple synergist (e, g., flexor or extensor) motoneuron pools. During deletions, the maintained activity of antagonist motoneuron pools usually becomes tonic or continue to be rhythmic (Lafreniere-Roula and McCrea 2005; Rybak et al. 2006a;
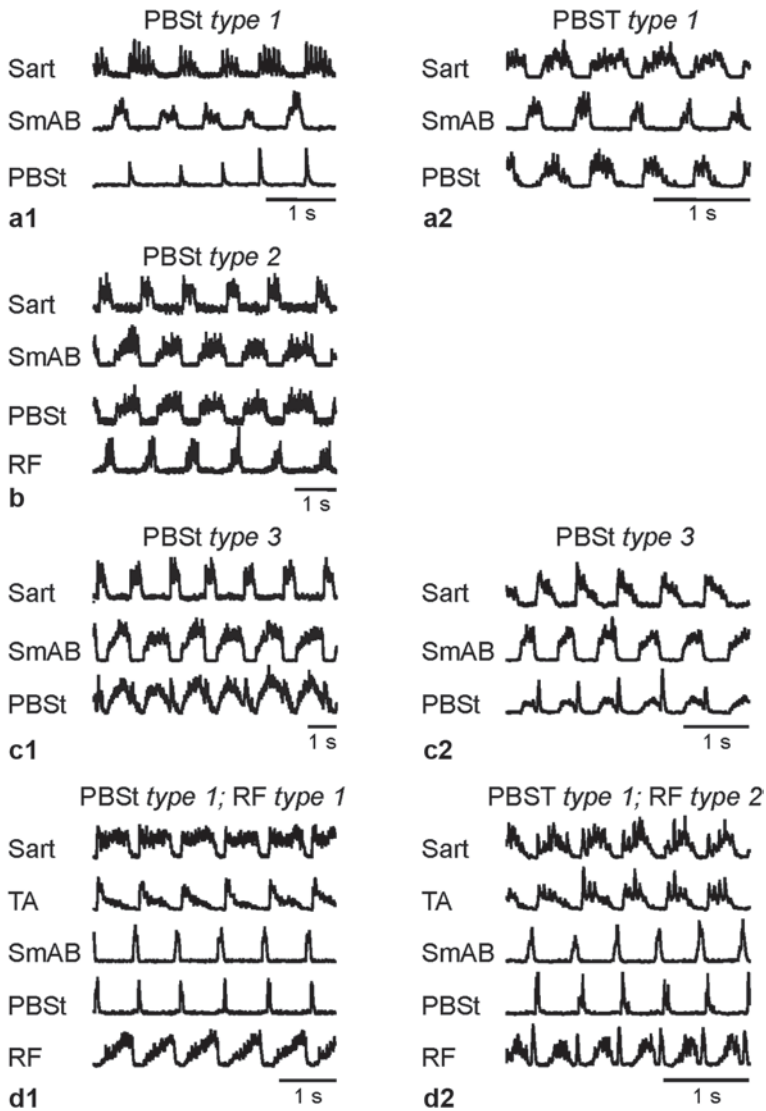
Fig. 5.3 Activities of the PBSt and RF motoneuron pools in selected fictive locomotion experiments. **a1, a2** The PBSt motoneuron pool (type 1) is active either at the onset of the flexor phase or during most of the flexor phase. **b** The PBSt motoneuron pool (type 2) is active in the extensor phase. **c1, c2** The biphasic PBSt ENG (type 3). **d1** The motoneuron pools of PBSt (type 1) and RF (type 1) are active in the flexor phase. **d2** The PBSt motoneuron pool (type 1) is active in the flexor phase, and the RF ENG (type 2) is biphasic
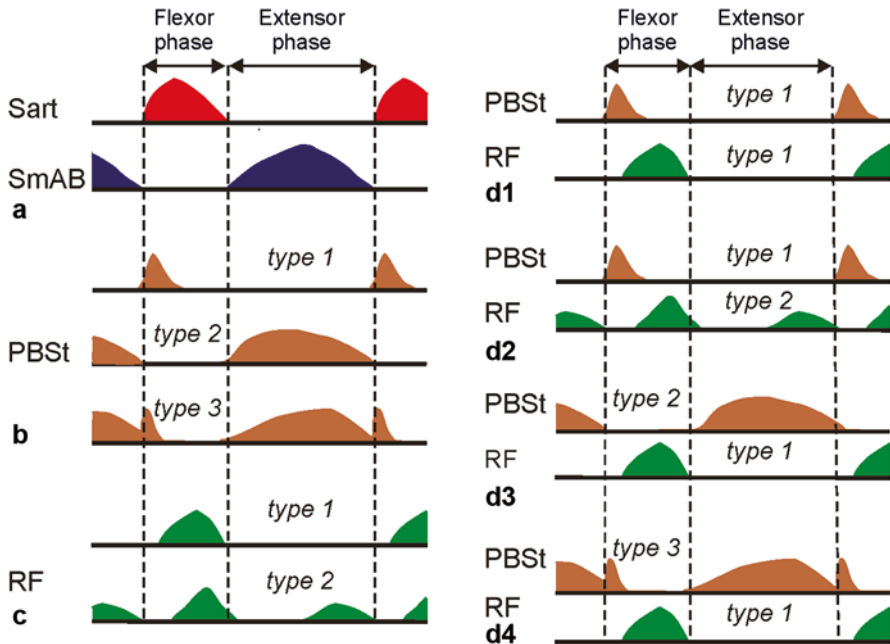
Fig. 5.4 Averaged and normalized patterns of PBSt and RF ENG activities with respect to flexor and extensor activity profiles during fictive locomotion. **a** Typical flexor (Sart) and extensor (SmAB) patterns. **b** Three patterns of PBSt motoneuron activities: type 1, the PBSt motoneuron pool is active at the beginning of the flexor phase; type 2, the PBSt motoneuron pool is active during the extensor phase; and type 3, the PBSt motoneuron pool is active in both phases. **c** Two typical RF ENG patterns: type 1, the RF motoneuron pool is active in the flexor phase, and type 2, the RF motoneuron pool is active in both phases. **d1–d4** Possible combinations of PBSt and RF ENG activities recorded simultaneously. Modified from (Markin et al. 2012)

Shevtsova 2015). Deletions have been previously classified into two types: *resetting* deletions, characterized by a shift in the phase of post-deletion rhythmic activity relative to the pre-deletion rhythm, and *non-resetting* deletions, after which the post-deletion rhythmic activity re-appears with no phase shift relative to a pre-deletion rhythm (Lafreniere-Roula and McCrea 2005; Rybak et al. 2006a; Shevtsova 2015).

One would expect that if before deletions PBSt or RF was active in one phase only (i.e., showed activity like a flexor or extensor), its behavior during the deletion would resemble the activity of the corresponding motoneurons (flexor or extensor). However, experimental data indicate that PBSt and RF behaviors during deletions have no direct correspondence with their pre- or post-deletion activity. For example, in three experiments shown in Fig. 5.5a–c, each episode contains a resetting extensor deletion (silence of SmAB, MG, Plant, LGS) accompanied by tonic activity of flexor motoneuron pools (Sart, TA). In all three episodes before and after deletion, PBSt demonstrates flexor-related activity (*type 1*). However, the behavior of PBSt during deletions in these episodes is completely different. In Fig. 5.5a, the PBSt motoneuron pool becomes tonically active during the deletion, i.e., behaves as the
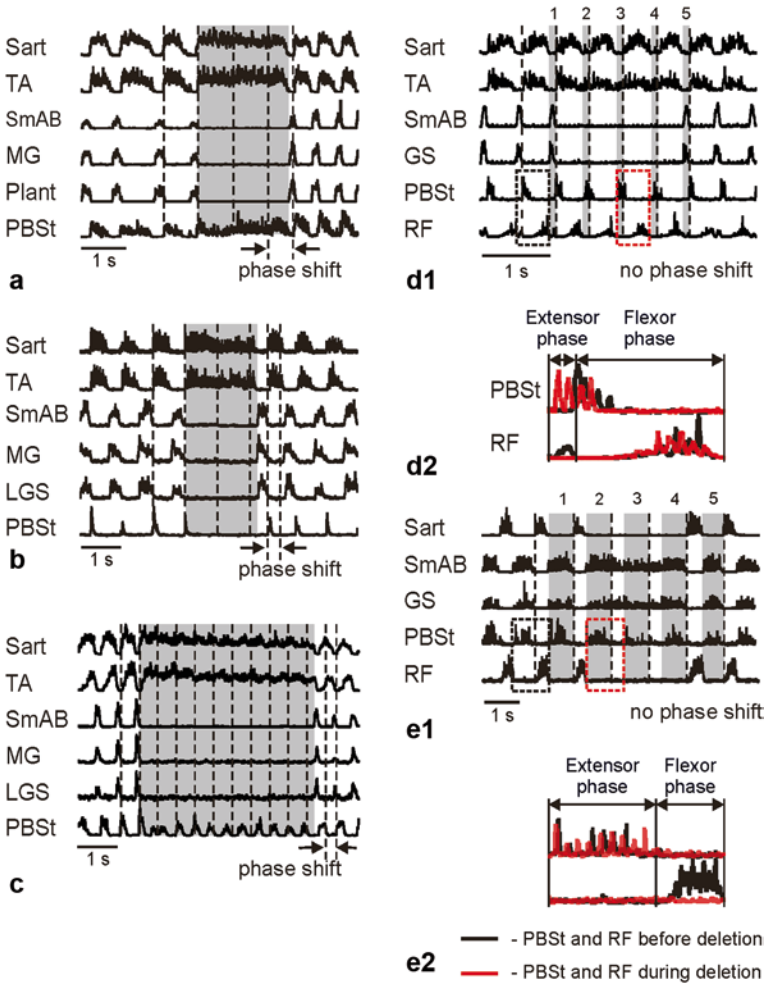
Fig. 5.5 a, b, c Examples of variable behavior of PBSt ENGs during resetting deletions of extensor activity (SmAB, MG, Plant, and LGS) accompanied by sustained activity in flexors (Sart and TA). In this and the following figures, the *vertical dashed lines* plotted at the intervals of an average locomotor period indicate the beginning of the flexor phases before and after deletions and the beginning of the expected flexor phases during deletions. In all three deletions shown in **a–c**, there is an obvious phase shift of the post-deletion rhythm with respect to the pre-deletion rhythmic activity (see arrows at the bottom) indicating that these deletions are resetting. In all three recordings in **a–c** PBSt ENG is of the flexor type before and after deletions. During deletions, the PBSt motoneuron pool demonstrates tonic activity like flexors in **a**, is silent like extensors in **b**, and expresses rhythmic activity in **c**. Note that frequency of PBSt ENG oscillations in **c** differs from the locomotor frequency before and after the deletion. **d1, e1** Examples of PBSt (**d1, e1**) and RF (**e1**) ENG activity during extensor (**d1**) and flexor (**e1**) deletions. The lack of phase shift of the post-deletion rhythmic activity with respect to the pre-deletion rhythm indicates that the deletions shown in panels **d1** and **e1** are non-resetting. **d2, e2** Enlarged and overlapped traces of PBSt and RF ENG activities during one locomotor period before (*black*) and during (*red*) the deletions outlined in **d1** and **e1** by *dashed* rectangles. Shaded rectangles in **d1** and **e1** highlight the extensor phases before and after the deletions and the expected extensor phases during the deletions

flexor motoneuron pools. In Fig. 5.5b, the PBSt motoneuron pool is silent during the deletion episode similar to extensor motoneurons. In Fig. 5.5c, the PBSt motoneuron pool expresses rhythmic activity during the deletion and the frequency of this activity differs from the locomotor frequency before and after the deletion.

Figure 5.5d1 shows an episode with a non-resetting extensor deletion (SmAB and GS are silent for some time interval). In this example before and after the deletion, PBSt is active in the flexor phase (*type 1*) like a typical flexor. During the deletion, however, PBSt remains rhythmic, and its activity becomes biphasic (see an expanded insert d2 showing two overlapped locomotor periods, one taken before and the other taken during the deletion).

Figure 5.5e1 shows an episode of fictive locomotion, in which PBSt normally expresses extensor-related activity (*type 2*), but during a non-resetting flexor deletion (Sart is silent) with tonically active extensors (SmAB and GS) PBSt remains rhythmically active.

To analyze a full specter of PBSt and RF behaviors during deletions, the experimental recordings containing PBSt and/or RF ENGs were classified according to the following characteristics: (a) type of agonist motoneuron pool (flexor or extensor) whose activity was missing during deletion; (b) deletion type (resetting or non-resetting, see Lafreniere-Roula and McCrea 2005; Rybak et al. 2006a; Shevtsova 2015), and were divided into groups based on the type of PBSt or RF pre- and post-deletion activity and their behavior during deletion (silent/tonic/rhythmic). This analysis (see Table 5.1) included data from 36 experiments. In some experiments, there were several deletion episodes separated by rhythmic locomotor activity. We noticed obvious differences in behavior of the flexor-type PBSt ENG with a short flexor burst (*type 1a*) vs. a longer flexor burst (*type 1b*) during most of deletions. Similarly, the behaviors of biphasic PBSt ENG with a short flexor burst and that with a longer flexor burst were also different during resetting extensor deletions. Though no data were found demonstrating biphasic PBSt ENG with a longer flexor burst for other types of deletions, we separated biphasic PBSt ENG patterns into two subgroups, *type 3a* and *3b* depending on the length of the flexor burst similar to the flexor-type PBSt. The results of our classification are summarized in Table 5.1. Numbers in parentheses in Table 5.1 indicate the numbers of episodes where the indicated behavior was observed during particular deletion types for each type of PBSt or RF ENG patterns. The re-appearing post-deletion activity patterns were the same as the pre-deletion patterns in the absolute majority of experiments.

5.3 Constructing the Extended CPG Model

5.3.1 Shaping Profiles of PBSt and RF Activity

Analysis of intracellular recordings from PBSt and RF motoneurons shows that they often exhibit depolarization in both locomotor phases, even if this depolarization is sufficient for firing during only one phase, flexor or extensor. This observa-

Table 5.1 Behavior of PBSt and RF ENGs during spontaneous deletions

	Deletion type				
	Extensor deletions			Flexor deletions	
	Tonic flexors		Rhythmic flexors	Tonic extensors	
	Resetting	Non-resetting		Resetting	Non-resetting
PBSt					
Flexor, short burst (*type 1a*)	Silent (7)	Rhythmic[a] (1)	Silent or rhythmic[a] (1)	Silent (4)	
Flexor, long burst (*type 1b*)	Tonic (4) or rhythmic[b] (1)	Rhythmic[c] (4)	Rhythmic (3)	Silent (4)	
Extensor (*type 2*)	Silent (9)		Silent (4)	Tonic (8)	Silent (1) or rhythmic[a] (1)
Biphasic, short flexor burst (*type 3a*)	Silent (7)		Silent (1)	Tonic (5)	Not found
Biphasic, long flexor burst (*type 3b*)	Tonic (2)	Not found			
RF					
Flexor (*type 1*)	Tonic (5)	Rhythmic (1)	Rhythmic (3)	Silent (7)	
Biphasic (*type 2*)	Tonic (5)	Rhythmic[d] (7)	Rhythmic[d] (9)	Not found	

[a] Amplitude of rhythmic activity is markedly reduced and some bursts are missing
[b] Frequency of PBSt ENG oscillations differs from the frequency before/after deletion
[c] Flexor-type PBSt ENG pattern becomes biphasic during deletions
[d] RF ENG pattern loses its extensor component

tion led to the suggestion that PBSt and RFs motoneurons receive excitatory inputs from both flexor and extensor half-centers of the CPG (Perret 1983; Orsal et al. 1986; Perret et al. 1988). Another suggestion of Perret et al. was the existence of additional excitatory and inhibitory interneuron populations interposed between the CPG and PBSt and RF motoneurons that shape their firing patterns. These suggestions were explicitly used in the construction of our model.

Figure 5.6 shows schematically the possible neural connectivity allowing shaping the activity profiles of PBSt and RF motoneurons. As suggested above, they receive excitatory inputs from both half-centers and additional inhibitory inputs from hypothetical interneuron populations shaping their activity. Panel A shows typical profiles of flexor (Sart) and extensor (SmAB) activities that may represent the profiles of excitatory input from flexor (red) and extensor (blue) half-centers, respectively. Figure 5.6b1–b5 schematically shows the net excitation that the PBSt and RF would receive from flexor and extensor half-centers (filled gray areas) superimposed with the typical PBSt (Fig. 5.6b1–b3, upper panels) or RF (Fig. 5.6b4, b5, upper panels) profiles. For each particular PBSt or RF pattern, we can see "extra excitation" that should be eliminated by some inhibitory inputs to the corresponding populations (lower panels in Fig. 5.6b1–b5, flexor- and extensor related components of the inhibitory signals are shown in red or blue, respectively). Figure 5.6c1–c5 schematically shows how each of PBSt and RF patterns can be sculptured by additional
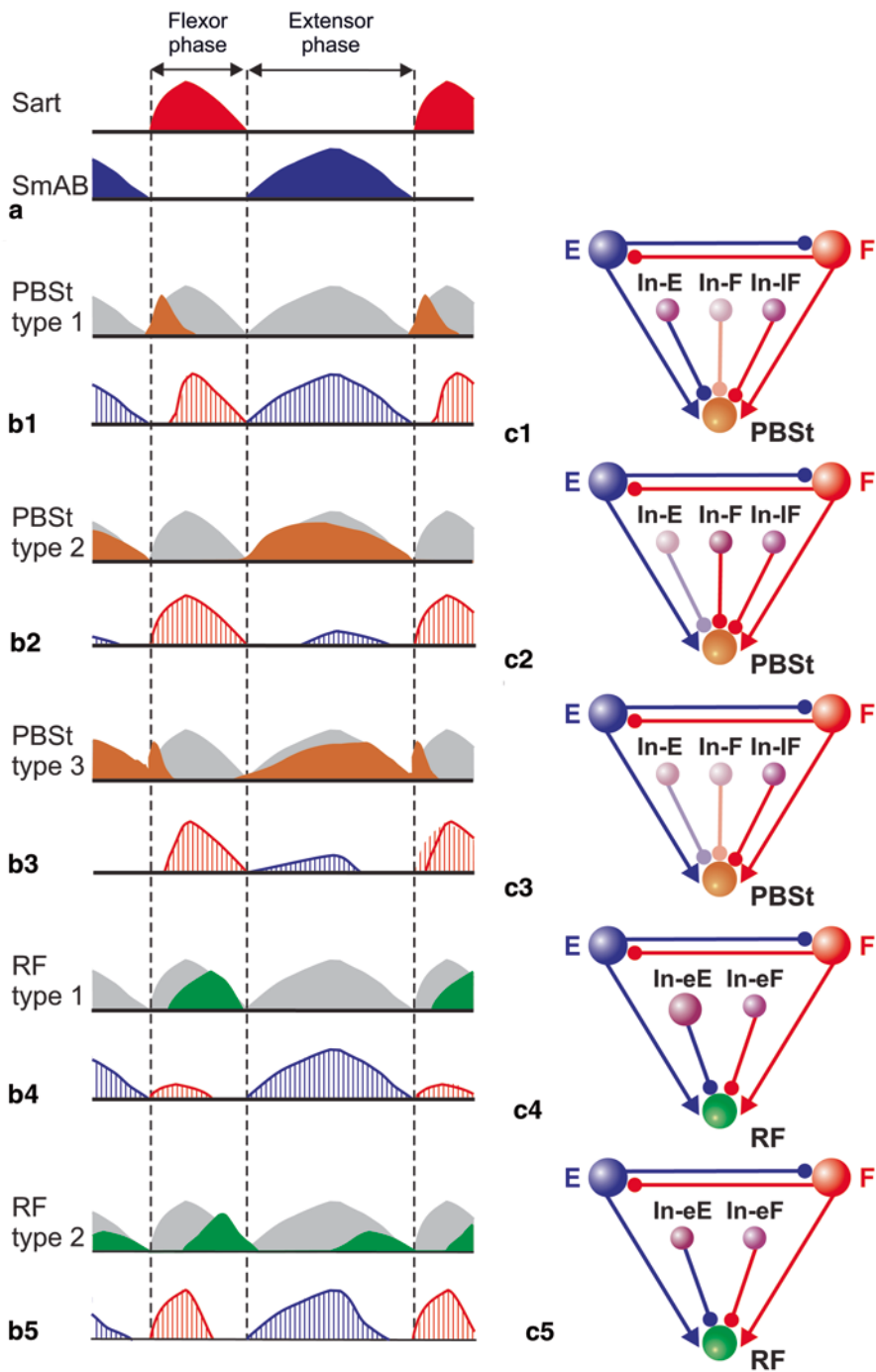
Fig. 5.6 Shaping PBSt and RF motoneuron activities of different types in fictive locomotion. **a** Averaged and normalized activities of typical flexor (Sart) and extensor (SmAB) motoneuron pools. **b1–b5** *Upper* traces, typical PBSt (**b1–b3**, *brown filled areas*) or RF (**b4** and **b5**, *green filled*

inhibitory interneuron populations. Specifically, PBSt activity in the extensor phase can be shaped by an extension-related inhibitory population, In-E, which is active throughout the extensor phase. If activation of this population is strong, the extensor component of PBSt activity will be fully inhibited (Fig. 5.6b1, c1). If activation of this population is moderate or weak, PBSt will maintain an extensor component and exhibit an extensor (Fig. 5.6b2, c2) or biphasic pattern (Fig. 5.6b3, c3). PBSt activity in the flexor phase can be controlled by an inhibitory population firing throughout the flexor phase, In-F. Strong activation of this population will result in complete suppression of the flexor component of PBSt activity (Fig. 5.6b2, c2); if the In-F population is silent or weakly activated, the PBSt motoneuron pool will demonstrate activity in the flexor phase (Fig. 5.6b1, c1, b3, c3). The length of the PBSt flexor burst can be regulated by an additional inhibitory population, active in a later part of the flexor phase, In-lF (Fig. 5.6b1, c1, b3, c3).

Similarly, the flexor component of RF profile can be shaped by two inhibitory populations: In-eF that shapes the RF activity during the flexor phase, and In-eE that shapes the extensor component of RF activity (Fig. 5.6b4, c4, b5, c5). Note that if the In-eE population is strongly activated, it becomes active during the whole extensor phase (see Fig. 5.6b4, c4). In this case the extensor component of RF activity will be fully suppressed and RF will exhibit a flexor-type activity (Fig. 5.6b4, c4); otherwise RF activity will be biphasic (Fig. 5.6b5, c5).

5.3.2 Basic Concept and PF Network Architecture

The ultimate goal of our modeling effort was to extend our basic two-level model of the spinal locomotor CPG (Rybak et al. 2006a) so that it could reproduce complex patterns of bifunctional motoneurons such as PBSt and RF. Similar to the preceding model, the extended model includes a bipartite RG and PF network. Also, similar to that model the locomotor activity is initiated by external tonic "MLR" drive to the excitatory neural populations of the CPG. This way to initiate the rhythm allowed us to perform direct simulation of fictive locomotion conditions.

While extending the basic two-level CPG model, we have suggested that the model reproduction of complex patterns of PBSt and RG motoneurons can be achieved by a special construction of pattern formation (PF) network without changing the

areas) activity patterns overlapped with summarized flexor and extensor activities (_gray filled areas_). Bottom traces, hypothetical inhibitory inputs shaping each type of PBSt and RF activity patterns and representing the difference between summarized flexor and extensor activities and the corresponding PBSt or RF profile. _Red_ and _blue patterned filled areas_ correspond to inhibitory influence on the PBSt and RF motoneurons in the flexor or extensor phase, respectively. **c1–c5** Hypothetical neural circuitries participating in shaping particular PBSt and RF patterns. Spheres marked by _E_ (_blue_) and _F_ (_red_) schematically represent the flexor and extensor parts of the CPG. _PBSt_ (_brown_) and _RF_ (_green_) populations are shown as larger spheres. Smaller spheres represent hypothetical inhibitory interneuron populations sculpting PBSt and RF activity profiles. Strength of neuron activation in populations is symbolically shown by level of brightness of the corresponding sphere. Larger size of the In-eE population in **c4** indicates a strong activation of this population during the whole extensor phase to shape the flexor-type RF. See text for details

bipartite organization of the RG. So, similar to the preceding model (Rybak et al. 2006a, see Fig. 5.2) the locomotor rhythm generation in the RG is based on a combination of intrinsic (persistent sodium current dependent) properties of the excitatory RG neurons, mutual excitation within each half-center (RG-F and RG-E populations) and reciprocal inhibition between the half-centers via the inhibitory interneuron populations (Inrg-F and Inrg-E, see Fig. 5.2). The alternating bursting activities of the RG-F and RG-E populations (half-centers) define the extensor and flexor phases of the locomotor cycle, respectively. The PF network contains the two principal PF populations (PF-F and PF-E) that also receive the MLR drive. They also receive excitatory inputs from the homonymous RG populations and inhibitory inputs from the interneuron populations (Inrg-F and Inpf-F, or Inrg-E and Inpf-E, correspondingly, see Fig. 5.2). The PF-F and PF-E populations transmit rhythmic activities to the flexor (Mn-F) and extensor (Mn-E) motoneuron populations, respectively, and to the homonymous inhibitory Ia populations, providing reciprocal inhibition between the flexor and extensor motoneuron populations. There are also populations of Renshaw cells (R-F and R-E) that receive collateral excitatory input from the corresponding motoneuron populations (Mn-F and Mn-E) and provide feedback inhibition to the homonymous motoneuron population and the population of Ia inhibitory neurons (Ia-F or Ia-E), rhythmically inhibiting motoneuron populations during the inactive phase of the locomotor cycle (Fig. 5.2). To control the populations of PBSt and RF motoneurons (Mn-PBSt and Mn-RF, respectively) we needed to incorporate in the PF network the principle PF-PBSt and PF-RF populations that would project to the Mn-PBSt and Mn-RF motoneuron populations and to organize interactions between the PF-PBSt and PF-RF and other CPG populations (Fig. 5.7).

According to this idea (and similar to the PF-F and PF-E populations), the PF-PBSt and PF-RF populations should receive the "MLR" drive. They should also receive excitatory inputs from both extensor and flexor parts of the CPG that could come from the RG and/or PF levels (i.e., from the RG-E or PF-E, and from the RG-F or PF-F populations). Additional inhibitory interneuron populations, that are necessary to sculpt the PBSt and RF activity (In-E, In-F, In-lF, In-eF, and In-eE, see Fig. 5.6), should be also included in the PF network and shape the activity of the PF-PBSt and PF-RF (and hence Mn-PBSt and Mn-RF) populations (purple small spheres and connections in Fig. 5.7a1, b1). To be active in a particular phase of the locomotor cycle (flexor or extensor), these additional populations should receive rhythmic excitatory inputs from either flexor or extensor side of the CPG at different levels (RG or PF). We suggested that to be active in a certain locomotor phase, these populations receive tonic excitatory drive and are inhibited in the opposite phase by inhibition from the corresponding Inrg or Inpf populations. To determine possible organization of inputs from RG and PF populations to the PF-PBSt, PF-RF and additional interneuron populations, we analyzed the activity of PBSt and RF during two non-resetting deletions shown in Fig. 5.5d1, d2. During this analysis, we took into account a previous suggestion (Rybak et al. 2006a) that non-resetting deletions result from perturbations (additional drives or increase of excitability) affecting only one side (flexor or extensor) of the PF network, while keeping rhythmic activity of the RG populations (see Table 5.2). The results of such logical approach are illustrated in Fig. 5.9.
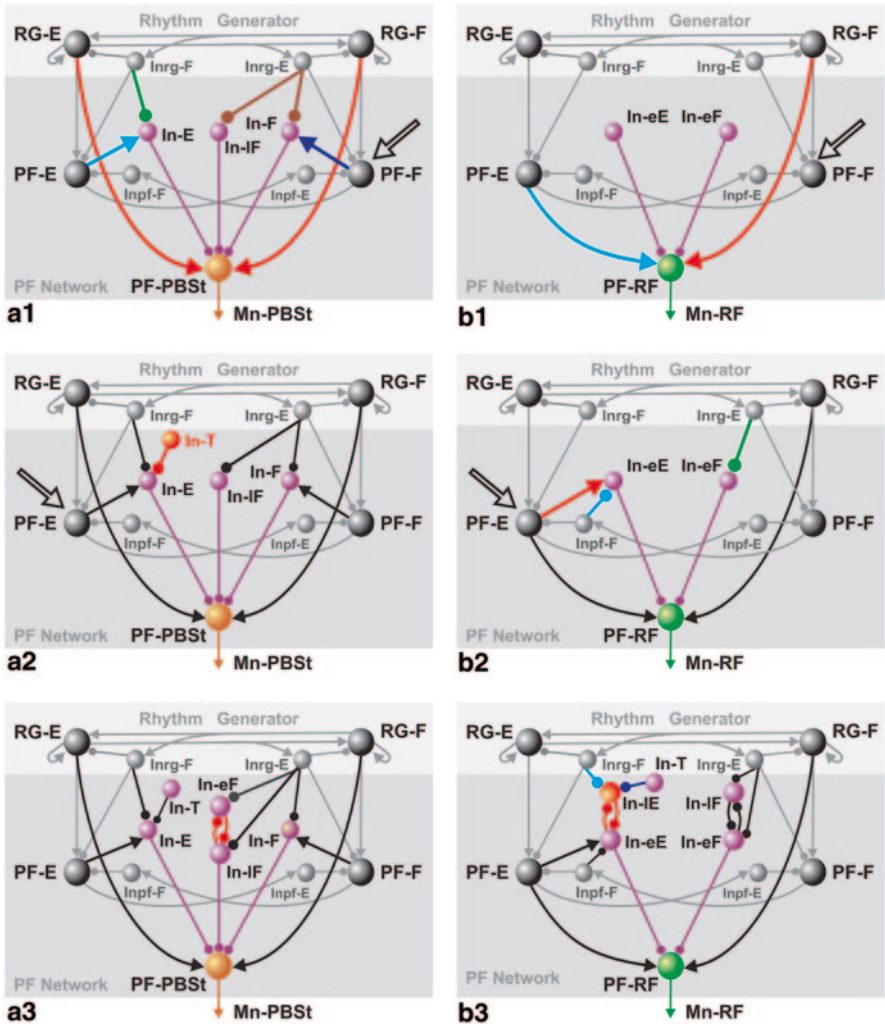
Fig. 5.7 Incorporating circuits controlling PBSt (**a1, a2**) and RF (**b1, b2**) motoneuron activities in the PF network on the base of analysis of fictive locomotion episodes with particular deletions shown in Fig. 5.5d1, e1. The *left column* (panels **a1** and **a2**) illustrates sequential building of PBSt circuitry. The *right column* (panels **b1** and **b2**) shows sequential construction of RF circuitry. At each step of circuitry construction newly introduced network elements are highlighted by particular color. **a3, b3** Extension of PF circuitries controlling the PF-PBSt (**a3**) and PF-RF (**b3**) populations behavior in the extended model to provide complimentary patterns of PBSt and RF activity. See details and explanations in the text

Let us first consider fictive locomotion recordings shown in Fig. 5.5d1. These recordings show a fictive locomotion episode with a non-resetting deletion of extensor activity. Since this deletion is non-resetting it may result from an increased excitation of the PF-F population that fully inhibits the PF-E population and hence produces a non-resetting deletion of extensor activity, while the RG-E and RG-F

populations maintain rhythmic activity (Rybak et al. 2006a). In Fig. 5.7a1, b1 this increase of excitation is schematically shown by large unfilled arrows to the PF-F population. During this extensor deletion, not all flexors switched to tonic activity: TA did switch and showed modulated sustained activity, whereas Sart remained rhythmically active.

In this experiment, before and after deletion, PBSt exhibited a flexor activity profile (*type 1b*) (see shaded bars 1 and 5 in Fig. 5.5d1 and black trace in Fig. 5.5d2). According to our suggestion the flexor-type PF-PBSt profile can be sculptured by activation of the In-E and In-lF populations (see Fig. 5.6c1). These inhibitory populations would inhibit the PF-PBSt population during the extensor phase and later in the flexor phase, respectively. In contrast, the In-F population that inhibits the PF-PBSt population in the flexor phase should be silent or weakly activated. As seen in Fig. 5.5d1, d2, during the deletion, the PBSt motoneuron pool remained rhythmically active, but its activity profile turned into biphasic; it started firing in the expected extensor phases and continued in the flexor phases. Such firing pattern during non-resetting extensor deletions is typical for PBSt (see Table 5.1) and allows several suggestions about possible organization of inputs from the RG and PF populations to the PF-PBSt and additional inhibitory interneuron populations (In-E, In-lF, and In-F):

1. Biphasic activity of PBSt during this deletion may indicate that the PF-PBSt population receives excitatory inputs from the RG-F and RG-E populations (see red bold connections in Fig. 5.7a1) that continue to be rhythmically active during this deletion (see Table 5.2).
2. PBSt activity that appears in the expected extensor phases may result from a reduction in activity of the In-E population during deletion allowing partial release of the PF-PBSt population from inhibition. Thus, the In-E population may receive excitatory input from the PF-E population (see blue bold connection in Fig. 5.7a1) that becomes silent during this deletion (Table 5.2).
3. To allow the PF-PBSt population to be active in the expected flexor phases during deletion, the In-E population should be inhibited by the Inrg-F population (green bold line in Fig. 5.7a1) that remains rhythmically active during non-resetting extensor deletions (Table 5.2).
4. Similarly, to allow PBSt activity during the expected extensor phases during this deletion, the In-F and In-lF populations should both be inhibited by the Inrg-E population (brown bold lines in Fig. 5.7a1) that remains rhythmically active during non-resetting extensor deletions (see Table 5.2).
5. During this deletion, PBSt may remain active at the beginning of the flexor phase but with reduced amplitude and duration (see the traces of PBSt activity before and during deletion in Fig. 5.5d2). This indicates that in addition to excitatory tonic input drive, the In-F population may receive a weak excitatory input from the PF-F population (dark blue bold line in Fig. 5.7a1) that increases its activity during non-resetting extensor deletion.

In experiment shown in Fig. 5.5d1, RF expresses biphasic activity (*type 2*) before and after deletion. According to our suggestion (see Fig. 5.6c5), the activity of

Table 5.2 Activity of CPG populations in the basic model during spontaneous deletions

Population name	Deletion type				
	Extensor deletions			Flexor deletions	
	Tonic flexors		Rhythmic flexors	Tonic extensors	
	Resetting	Non-resetting	Non-resetting	Resetting	Non-resetting
RG-E/Inrg-E	Silent	Rhythmic	Rhythmic	Tonic	Rhythmic
RG-F/ Inrg-F	Tonic	Rhythmic	Rhythmic	Silent	Rhythmic
PF-E/ Inpf-F	Silent	Silent	Silent	Tonic	Tonic
PF-F/ Inpf-F	Tonic	Tonic	Rhythmic	Silent	Silent

biphasic RF can be sculptured by activation of the In-eE and In-eF populations, inhibiting the PF-RF population during the beginning of the extensor and flexor phases, respectively. During this deletion (and other similar deletions, see Table 5.1), RF remains rhythmically active in the expected flexor phases, but loses its extensor component. Such firing pattern of biphasic RF during non-resetting extensor deletions allows the following suggestions about organization of inputs from the RG and PF populations to the PF-RF population and interneuron populations incorporated to shape RF activity (In-eE and In-eF):

1. The PF-RF population may receive an excitatory input from the RG-F population (red bold line in Fig. 5.7b1) that continues to be rhythmically active during this deletion (see Table 5.2).
2. The PF-RF population may receive excitatory input from the PF-E population (blue bold line in Fig. 5.7b1) that becomes silent during non-resetting extensor deletions (Table 5.2).

Let us now consider a fictive locomotion episode with a non-resetting deletion of flexor activity (missing activity of Sart) shown in Fig. 5.5e1. During such deletions, the RG-E and RG-F populations may maintain rhythmic activity, while the PF-E population would show sustained tonic activity and the PF-F population would become silent (Rybak et al. 2006a). Such deletion in the model may result from increasing excitation of the PF-E population (Rybak et al. 2006a) shown by the large unfilled arrows to the PF-E population in Fig. 5.9a2, b2.

In episode shown in Fig. 5.5e1, before and after deletion PBSt was active during the extensor phase and silent during the flexor phase (*type 2*). To provide shaping of such PBSt pattern, the In-F population that inhibits the PF-PBSt population during the flexor phase should be strongly activated, while the In-E population inhibiting the PF-PBSt population in the extensor phase should be weakly active or silent. According to our suggestion above, the In-E population receives excitatory input from the PF-E population (see Fig. 5.7a1, blue bold connection). Thus, to suppress activity of the In-E population and allow PBSt to be active in the extensor phase, an In-T population is included in the model that receives tonic excitatory input and inhibits the In-E population (shown by red in Fig. 5.7a2). Hence, the activity of the In-T population controls the In-E (and hence PF-PBSt) population activity during the extensor phase. Specifically, if the In-T is silent, the In-E population is

strongly activated and inhibits the PF-PBSt population in the extensor phase. In contrast, if the In-T population is strongly activated, it inhibits the In-E population, thus allowing the PF-PBSt population activity in the extensor phase. Finally, if the In-T population is moderately activated, the In-E population expresses a moderate activity in the extensor phase and the PF-PBSt population would exhibit a reduced extensor activity.

During the deletion shown in Fig. 5.5e1, PBSt rhythmic activity persists in the expected extensor phases (see shaded bars 2–3 in Fig. 5.5e1 and overlapped traces in Fig. 5.5e2), although reduced relative to its activity before and after deletion. This supports our suggestion that the In-E population receives an excitatory synaptic input from the PF-E population (Fig. 5.7a1, blue bold connection) whose activity increases during this and similar deletions. Evidently, during the deletion shown in Fig. 5.5e1, the In-F population remains rhythmically active and inhibits the PF-PBSt population activity during the expected flexor phase, supporting our previous suggestion that in addition to the excitatory tonic drive this population may receive an inhibitory synaptic input from the Inrg-E population (Fig. 5.7a1, dark blue bold connection).

In the experimental recordings shown in Fig. 5.7e1, RF expressed flexor activity (*type 1*) before and after a non-resetting extensor deletion. Such RF pattern may be sculptured by activation of the In-eF populations at the beginning of the flexor phase and by the In-eE population during the extensor phase (Fig. 5.6c4). During the deletion, RF became silent, which allows the following suggestions:

1. The In-eE population inhibiting the PF-RF population during the extensor phase may be excited by the PF-E population (see red bold connection in Fig. 5.7b2) that becomes tonic and increases its activity during such deletions (see Table 5.2).
2. The In-eE population is inhibited by the Inpf-F population (blue bold connection in Fig. 5.7b2) that becomes silent during such deletions (see Table 5.2).

To complete organization of connections to populations shaping RF activity we suggested that the In-eF population is inhibited by the Inrg-E population (green bold connection in Fig. 5.7b2).

Inhibitory interneuron populations (In-lF, In-eF, and In-eE) incorporated in the PF network to shape PF-PBSt and PF-RF activity (Figs. 5.6 and 5.7) should be active either in the beginning ("early" type, e.g., In-eF or In-eE) or in the later part of the corresponding phase ("late" type, In-lF). To shape such activity patterns, we suggested that neurons with an "early" pattern of activity have intrinsic adaptive properties and that neurons with the "late" pattern of activity in the In-lF population are inhibited by the neurons of the "early" type in the In-eF populations. In addition, we suggested that the In-lF and In-eF populations mutually inhibit each other, thus providing complimentary activity patterns of the In-eF and In-lF populations and hence, complimentary shaping of the of PBSt and RF activity profiles during the flexor phase (Fig. 5.7a3, red connections). To provide complimentary shaping PF-PBSt and PF-RF activities in extension, we incorporated in the PF network an In-lE population (shown in red in Fig. 5.7b3) that is active in late extension, receives an excitatory tonic drive, and is inhibited by the Inrg-F populations (blue connection

in Fig. 5.7b3). We also suggested that similarly to the In-eF and In-lF populations, the In-eE and In-lE populations mutually inhibit each other (red connections in Fig. 5.7b3). Finally, we suggested that in addition to tonic drive, activity of the In-lE population is regulated by inhibition from the In-T population (dark blue connection in Fig. 5.7b3) which controls activity of the PF-PBSt population in the extensor phase (see Fig. 5.7a2). If this inhibition is strong, it "prohibits" activation of the PF-RF population (by disinhibition of the In-eE population which inhibits the PF-RF activity) and "allows" the PF-PBSt activity (by inhibition of the In-E population and hence disinhibition of the PF-PBSt population) during the extensor phase. Thus, the In-T population provides complimentary shaping of the profiles of PF-PBSt and PF-RF activities during the extensor phase.
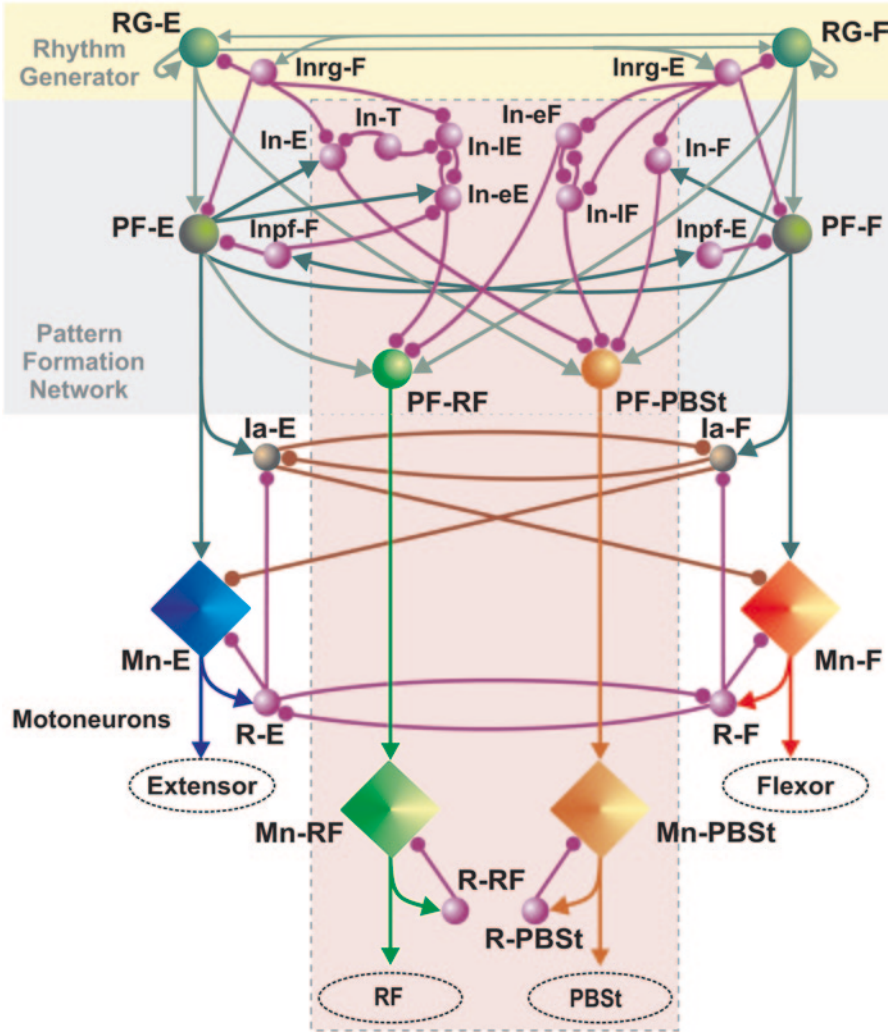
5.3.3   Extended Model

5.3.3.1   Model Architecture

Figure 5.8 shows the schematic of the extended model that includes all populations and circuits that were incorporated in the PF network of the CPG (see Figs. 5.6 and 5.7) to provide the full repertoire of PBSt and RF ENG activity profiles observed during fictive locomotion and their variable behavior during spontaneous deletions. In this model, activation of several inhibitory interneuron populations (In-E, In-T, In-F, In-eF, In-lF, In-eE, and In-lE) by tonic drives controls shaping of the PBSt and RF activity patterns and their behavior during deletions. The extended model also incorporates the motoneuron populations, Mn-PBSt and Mn-RF, and the populations of Renshaw cells, R-PBSt and R-RF, which receive collateral excitatory inputs from, and provide inhibitory feedback to, the homonymous motoneuron populations (Mn-PBSt and Mn-RF). Little data are available to conclude which motoneuron pools can be considered the direct antagonists of PBSt or RF motoneuron pools and if reciprocal interactions exist between the PBSt or RF motoneurons and some other motoneuron populations. Therefore, Ia-mediated reciprocal inhibition to and from PBSt and RF motoneurons was not included in the current version of the extended model.

5.3.3.2   Modeling Single Neurons and Neural Populations

All neurons were modelled in the Hodgkin-Huxley style. Interneurons were simulated as single-compartment models. Motoneurons had two compartments: soma and dendrite. The single neuron models were previously described in detail (Rybak et al. 2006a). A brief description of these neuron models, ionic currents included in each neuron type, and all model parameters are provided in the Appendix.

Each interneuron population included 20 neurons. Each motoneuron population had 40 neurons. Connections between populations were established such that, if

Fig. 5.8 Schematic of the extended model of the locomotor CPG. The model includes all populations of the basic CPG model (see Fig. 5.2) and an extension to simulate generation of PBSt and RF motoneuron activities (outlined by *pink rectangle*) that includes hypothetical circuitry incorporated into the PF network to control PBSt and RF behavior (see Figs. 5.6 and 5.7), two bifunctional motoneuron populations, Mn-PBSt and Mn-RF, and two populations of Renshaw cells, R-PBSt and R-RF, which receive collateral excitatory input from and provide feedback inhibition to the Mn-PBSt and Mn-RF populations, respectively. Note that all populations in the Rhythm Generator and Pattern Formation Network receive excitatory tonic drives (not shown)

a population A was assigned to receive an excitatory or inhibitory input from a population B or external drive d, then each neuron of population A received the corresponding excitatory or inhibitory synaptic input from each neuron of population B or from drive d, respectively. All connections were randomly distributed to provide

heterogeneity of individual neuron behavior in populations. The mean weights of synaptic connections between the neural populations in our model are shown in the Appendix (Table 5.A2). The standard deviation (SD) of synaptic weights varied from 10–15 % of the mean value.

The heterogeneity of neurons within each population was also provided by random distribution of the reversal potential of leak channel, E_L (see mean values ± SD in Appendix), initial conditions for values of the membrane potential, calcium concentrations and some channel conductances. In each simulation, a settling period of 20 s was allowed before data were collected. Each simulation was repeated 20–30 times, and demonstrated qualitatively similar behavior for particular mean values and standard deviations of distributed parameters.

All simulations were performed on a Dual Core Opteron(tm), 2.61 GHz/2.0 GB (DELL) with a Windows XP operating system using a special simulation package NSM 2.1 RC2, developed at Drexel University by I. A. Rybak, S. N. Markin, and N. A. Shevtsova using Microsoft Visual C++. Differential equations were solved using the exponential Euler integration method (MacGregor 1987) with a step of 0.1 ms (for details see Rybak et al. 2006a).

5.4   Model Performance

5.4.1   Sculpting PBSt and RF Activity Patterns

Similar to the original model by (Rybak et al. 2006a), the locomotor rhythm in the extended model is generated by the bipartite rhythm generator (RG). The alternating rhythmic bursts in flexor and extensor RG half-centers (RG-F and RG-E traces in Fig. 5.9a) define the durations of the extensor and flexor phases and hence the locomotor cycle period. At the PF level, the PF-F and PF-E populations follow the activity of the corresponding RG populations (see corresponding traces in Fig. 5.9). As shown in Fig. 5.8, the PF-PBSt and PF-RF populations project to the corresponding motoneuron populations (Mn-PBSt or Mn-RF, respectively) and receive excitatory synaptic inputs from both the RG-F and RG-E (for PBSt) or from the PF-E and RG-F (for RF) populations. The total synaptic drive to PF-PBST and PF-RF is shaped by a number of inhibitory interneuron populations (In-E, In-T, In-F, In-eF, In-lF, In-eE, and In-lE). For each type of PBSt and RF patterns, the activity of inhibitory interneuron populations (five upper traces in Fig. 5.9b1–b5) depends on tonic drive to each of these populations (d_E, d_T, d_F, d_{eF}, d_{lF}, d_{eE}, and d_{lE}, respectively, see Fig. 5.9c1–c5). The resulting activities of the PF-PBSt or PF-RF populations (and, respectively, Mn-PBSt or Mn-RF populations shown at the bottom in Fig. 5.9b1–b5) for each particular activity pattern depend on relative strength of the corresponding input drives (d_E, d_T, d_F, d_{eF}, d_{lF}, d_{eE}, d_{lE}).

Flexor-type Profile of PBSt Activity Figure 5.9b1, c1 illustrates sculpting the flexor-type PBSt activity pattern (type 1) in the extended model. To generate this
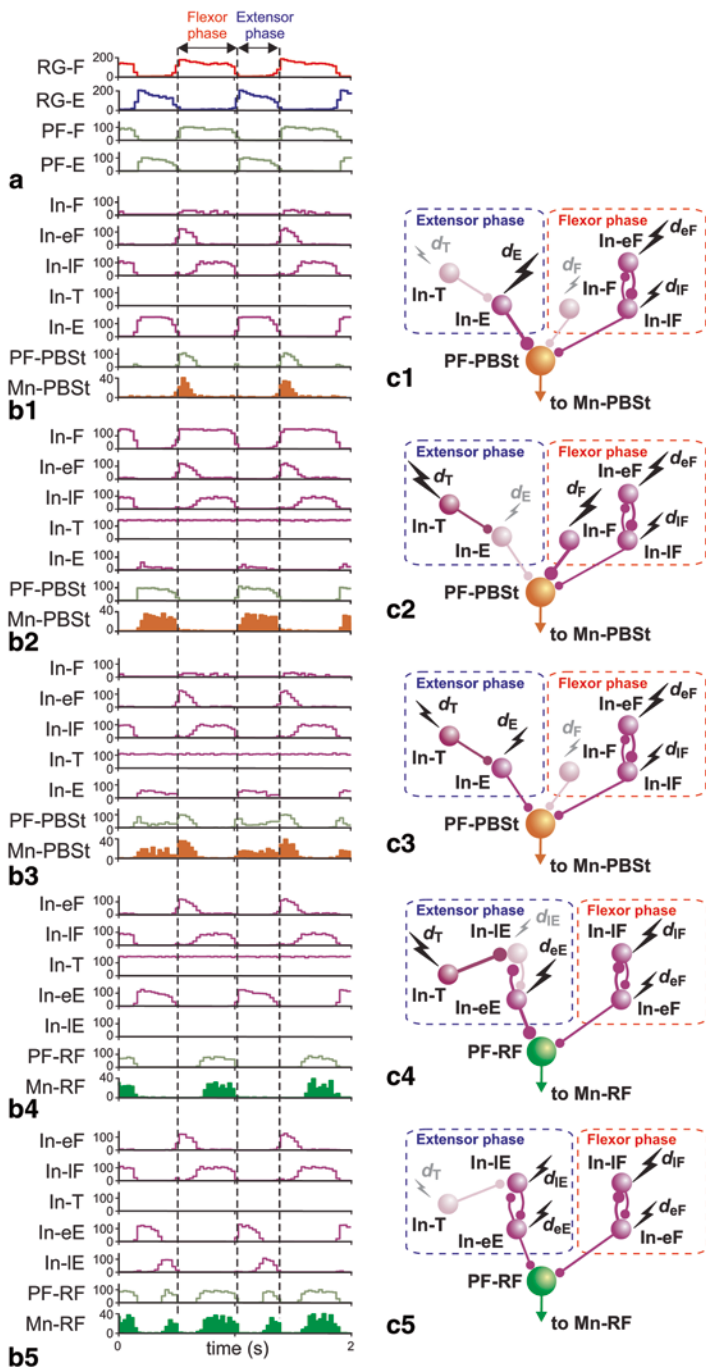
Fig. 5.9 Sculpting PBSt and RF motoneuron activity patterns in the extended model. The left column shows results of computer simulation for different PBSt and RF ENG activity types. Each trace represents a histogram of average neuron activity in a particular population (spikes

pattern, the PF-PBSt population should be inhibited during the extensor phase by the strongly activated In-E population and during later part of the flexor phase by the In-lF population. Activity of the In-E population depends on the excitatory tonic drive, d_E, and inhibition from the In-T population controlled by the tonic drive, d_T. Thus, if d_T is weak and d_E is strong enough (see Fig. 5.9c1), the In-E population will be strongly activated and fully suppress the activity of PF-PBSt (and hence Mn-PBSt) population during the extensor phase. At the same time, the In-F population, controlled by the tonic drive, d_F, should be silent or weakly activated to allow activity in PBSt motoneurons in the flexor phase, i.e., d_F should be weak. Duration of PBSt flexor bursts is defined by the activity of the In-eF and In-lF populations, inhibiting each other, and finally by tonic drives to these populations, d_{eF} and d_{lF}, respectively (see Fig. 5.9c1): the stronger d_{lF} and/or the weaker d_{eF} is, the shorter is the duration of PBSt flexor burst. Figure 5.9b1 shows activities of the In-T, In-T, In-F, In-eF, and In-lF populations shaping the flexor-type of PF-PBSt and hence Mn-PBSt profiles of activity.

Extensor-type Profile of PBSt Activity Figure 5.9b2, c2 shows shaping of the extensor type PBSt activity pattern (type 2). In case of the extensor type of PBSt profile, activity of PF-PBSt during the extensor phase should not be inhibited, i.e., the In-E population should be weakly activated or silent, which may occur when d_E is weak and/or d_T is strong enough (see Fig. 5.9c2). At the same time, the PF-PBSt activity during the flexor phase should be completely inhibited by the In-F population, i.e., d_F should be strong (Fig. 5.9c2). Figure 5.9b2 shows activities of the In-E, In-T, In-F, In-eF, and In-lF populations shaping the extensor-type of PF-PBSt and hence Mn-PBSt profiles of activity.

Biphasic Profile of PBSt Activity Figure 5.9b3, c3 illustrates shaping the biphasic type PBSt pattern (type 3). The biphasic PBSt profile includes a persistent activity (usually reduced) during the extensor phase followed by a short burst at the begin-

---

per neuron per second, bin = 30 ms). The right column shows neural circuits shaping different activity patterns. The rectangles outlined by *dashed lines* indicate populations participating in shaping activity of the PF-PBSt and PF-RF populations (*large green spheres*) during the flexor (*red*) or extensor (*blue*) phase. Small spheres represent inhibitory populations sculpting the PBSt and RF activity profiles. The bolts of different sizes schematically show strengths of excitatory input drives to inhibitory interneuron populations, the larger the bolt size, the stronger the input drive. Strength of neuron activation in a particular population is symbolically shown by thickness of output connection, the greater the level of excitation, the thicker the connection. Silent or weakly activated populations and their outputs are shown by lower brightness of the corresponding sphere or connection. **a** Alternating rhythmic bursts of the RG-F and RG-E populations (*two upper traces*) define locomotor cycle period and durations of the flexor and extensor phases (indicated by *vertical dashed* lines for one locomotor period). Two lower traces represent activities of the PF-F and PF-E populations, following activity of the corresponding RG populations. **b1–b5** Upper five traces represent activities of inhibitory interneuron populations shown in **c1–c5** and sculpting the flexor-type PBSt, type 1 (**b1, c1**); extensor-type PBSt, type 2 (**b2, c2**); biphasic PBSt, type 3 (**b3, c3**); flexor-type RF, type 1 (**b4, c4**); and biphasic RF, type 2 (**b5, c5**) activities. The last four traces in **b1–b5** show activity of the PF-PBSt or PF-RF populations and resulting activity of the corresponding motoneuron population (Mn-PBSt or Mn-RF, respectively). For values of input drives to the RG-F, RG-E, and hypothetical interneuron populations see Table 5.A3 in Appendix

ning of the flexor phase. In case of this profile, the reduced activity during the extensor phase can be provided by moderate inhibition of the PF-PBSt population by the In-E population; the level of inhibition here can be defined by the relative strengths of the tonic drives d_E and d_T to the In-E and In-T populations, respectively (see Fig. 5.9c3). The In-F population in this case should be silent or weakly activated to allow PF-PBSt activity in the flexor phase, i.e., d_F should be weak or absent (see Fig. 5.9c3). The duration of PBSt flexor bursts for the biphasic PBSt pattern is defined by relative activation of the In-eF and In-lF populations similar to the flexor-type PBSt pattern, and finally by the tonic drives d_{eF} and d_{lF} (see Fig. 5.9c3). Activities of the In-E, In-T, In-F, In-eF, and In-lF populations shaping the biphasic PBSt motoneuron activity pattern and the resulting PF-PBSt and Mn-PBSt activity profiles are shown in Fig. 5.9b3.

Flexor-type Profile of RF Activity Shaping the flexor-type RF profile of activity (type 1) is shown in Fig. 5.9b4, c4. In this case, the PF-RF population should be inhibited during the extensor phase and at the beginning of the flexor phase. In the model, whether or not the PF-RF population is active in the extensor phase is determined by activation of the In-eE population that depends on relative strengths of the tonic input drives d_{eE} and d_{lE} to the In-eE and In-lE populations, respectively (see Fig. 5.9c4), and on activation of the In-T population, i.e., on the tonic drive d_T. If d_{eE} and/or d_T are strong enough and d_{lE} is weak or absent, the In-eE population is active throughout the whole extensor phase and inhibits PF-RF activity during the extensor phase. Simultaneously, the PF-RF population is inhibited by the In-eF population at the beginning of the flexor phase, which depends on tonic drive d_{eF} and interaction between In-eF and In-lF populations, i.e., on the interplay between the tonic drives d_{eF} and d_{lF}. Figure 5.9b4 shows activities of the In-T, In-eE, In-lE, In-eF, and In-lF populations shaping the flexor-type PF-RF and Mn-RF activity profiles.

Biphasic Profile of RF Activity Figure 5.9b5, c5 illustrates shaping of the biphasic profile of RF activity (type 2). In this case, the PF-RF population should be inhibited at the beginning of the extensor phase and at the beginning of the flexor phase. Shaping RF activity later in the flexor phase for the biphasic RF activity is similar to that for the flexor-type RF activity (see above). To allow RF to generate an additional burst in the extensor phase, the tonic drive d_T to the In-T population should be weak (if present), and at the same time, the tonic drive d_{lE} to the In-lE population should be strong enough to overcome inhibition of this population by the In-eE population. In other words, if d_{lE} is strong enough, at some moment during the extensor phase the In-lE population escapes inhibition from the In-eE population and suppresses its activity by the end of the extensor phase. This allows the emergence of a short extensor burst in the PF-RF (and hence in Mn-RF) population during the later part of the extensor phase. Activities of the In-T, In-eE, In-lE, In-eF, and In-lF populations shaping the biphasic RF activity pattern and the resulting PF-RF and Mn-RF activities are shown in Fig. 5.9b5.

Figure 5.10 shows the results of our simulations for different types of PBSt and RF activities recorded during fictive locomotion experiments. Experimental recordings are shown for one flexor (Sart), one extensor (SmAB), PBSt, and RF (panels a1, b1, c1, and d1). The simulated traces (in panels a2, b2, c2, and d2, respective-

ly) show averaged frequency of spiking including (from top to bottom): the flexor (Mn-F), extensor (Mn-E), PBSt (Mn-PBSt), and RF (Mn-RF) motoneuron populations. In Fig. 5.10a1, PBSt has a flexor-type profile and RF shows a biphasic profile. The corresponding simulation is shown in Fig. 5.10a2. In Fig. 5.10b1, PBSt is also active in the flexor phase, but demonstrates a longer flexor burst, which is simulated in Fig. 5.10b2. In this simulation, the Mn-RF population also shows flexor-type activity profile, complimentary to the activity profile of the Mn-PBSt population. Figure 5.10c1 shows the experimental records, in which the PBSt demonstrates extensor-type of activity profile and the RF motoneuron pool is active in the flexor phase. This is simulated in Fig. 5.10c2. In Fig. 5.10d1, PBSt is biphasic and the RF ENG is of the flexor type. This is simulated in Fig. 5.10d2.

5.4.2 Modeling PBSt and RF Behavior During Deletions

5.4.2.1 Resetting Deletions

While developing the extended model, the challenge was not only to reproduce the full repertoire of PBSt and RF activity patterns observed in experimental studies but also explain their variable behavior during deletions (see Table 2.1). This specifically concerns the PBSt with a typical flexor-type activity profile that nevertheless during resetting extensor deletions can demonstrate tonic, silent, or rhythmic activity (Fig. 5.5a–c). According to the two-level concept of the CPG organization, resetting extensor deletions can be produced by either spontaneous increase of excitation of the flexor half-center (RG-F) or decrease in excitation of the extensor half-center (RG-E) (Rybak et al. 2006a). In the model, such deletion can be produced by a temporal change in the MLR drive to the corresponding RG population. During resetting extensor deletion, all major extensor-related populations become silent while flexor-related populations demonstrate sustained activity (see Table 5.2). Figure 5.11 demonstrates our simulations of variable behavior of the flexor-type PBSt during resetting extensor deletions shown in Fig. 5.5a–c. In order to have a flexor-type activity profile before and after deletions, the PF-PBSt population should be strongly inhibited during extension by the In-E population (see Fig. 5.9b1, c1). Besides, PF-PBSt activity during the flexor phase is controlled by inhibition from the In-lF population. The length of the PBSt flexor bursts before and after deletions depends on relative activation of the In-eF and In-lF populations, inhibiting each other, i.e. on the interplay between the excitatory tonic drives to these populations (d_{eF} and d_{lF}, respectively). During resetting extensor deletions, the PF-PBSt population receives a sustained excitation from the RG-F population shown by large unfilled arrows in Fig. 5.11a1–a3. The activity of In-E population is weak because it loses an excitatory input from the PF-E population and becomes tonically inhibited by the Inrg-F population (see Table 5.2). Both In-eF and In-lF populations lose inhibition from the Inrg-E population that becomes silent during resetting extensor deletions (see Table 5.2) and their behavior depends on the tonic drives to these populations (d_{eF} and d_{lF}, respectively) and mutual inhibition between
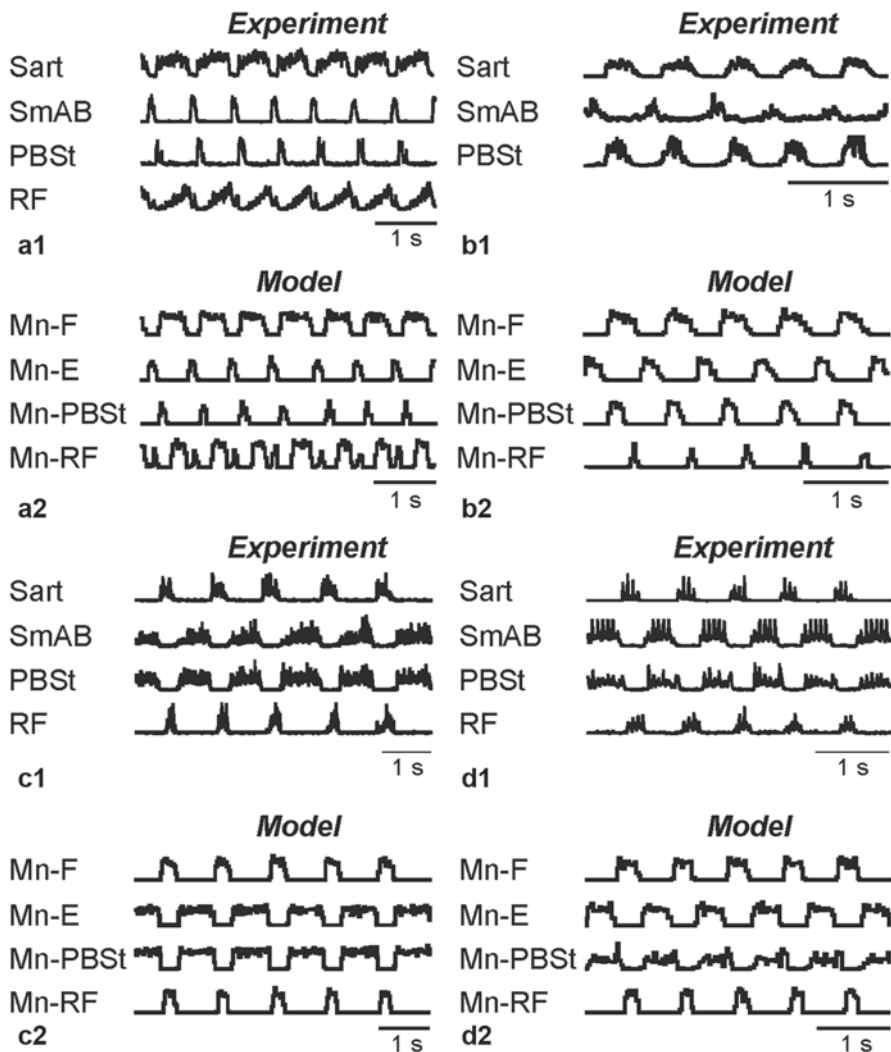
Fig. 5.10 Simulation of different types of the PBSt and RF ENG activities recorded during fictive locomotion experiments in the extended CPG model. Panels **a1**, **b1**, **c1**, and **d1** show recordings of the flexor (Sart), extensor (SmAB), PBSt, and RF ENGs. Panels **a2**, **b2**, **c2**, and **d2** show simulated activities of the Mn-F, Mn-E, Mn-PBSt, and Mn-RF populations as histograms of average neuron activity in a particular population (spikes per neuron per second, bin = 30 ms). **a1, a2** Flexor-type PBSt (type 1) and biphasic RF (type 2) motoneuron activity patterns. **b1, b2** Flexor-type PBSt and RF motoneuron activity patterns (both type 1, RF is shown in **b2** only). **c1, c2** Extensor-type PBSt (type 2) and flexor-type RF (type 1) motoneuron activity patterns. **d1, d2** Biphasic PBSt (type 3) and flexor-type RF (type 1) motoneuron activity patterns. For values of input drives to the RG-E, RG-E, and hypothetical interneuron populations see Table 5.A3 in Appendix

them. Mini-circuitries in Fig. 5.11a1–a3 schematically show how the interplay between d_{eF} and d_{lF} affects the PF-PFSt and Mn-PBSt behavior during resetting extensor deletions. Figure 5.11b1–b3 shows the corresponding simulations.

In Fig. 5.11b1, the flexor-type PBSt motoneuron population is active during most of the flexor phase (type 1b) before and after the deletion and demonstrates sustained activity during the deletion, similar to the experimental recordings shown in Fig. 5.5a. To demonstrate a prolonged flexor burst, the PF-PBSt population should be inhibited by the In-lF population at the very end of the flexor phase. This can be achieved if the In-lF population receives a weaker excitatory input drive d_{lF} compared to the drive d_{eF} to the In-eF population (see Fig. 5.11a1) that in this case is active during most of the flexor phase. During the deletion the In-eF population becomes tonically active and inhibits the In-lF population allowing tonic activity of the PF-PBSt population (and hence Mn-PBSt) as can be seen in Fig. 5.11b1. Alternatively, if d_{lF} is strong compared to d_{eF} (see Fig. 5.11a2), which is expected for the short flexor-type PBSt activity profile (type 1a), the In-lF population inhibits the In-eF population during most of the flexor phase before and after the deletion. During the deletion, this population loses inhibitory input from the Inrg-E population, becomes tonically active, and inhibits the PF-PBSt population, resulting in the silent Mn-PBSt population (Fig. 5.11b2). This behavior is similar to the experimental recordings shown in Fig. 5.5b. Finally, in some situations the mutual inhibition between the In-eF and In-lF populations can produce rhythmic activity with a frequency independent of the locomotor frequency before and after deletion (see the corresponding traces in Fig. 5.11a3). In this case, the resulting activity of the PF-PBSt and Mn-PBSt populations becomes rhythmic as seen in Fig. 5.11b3. This can explain rhythmic PBSt activity in experimental records shown in Fig. 5.5c.

Figure 5.12 shows experimental recordings (panels a1, b1, c1, and d1) and our simulations (panels a2, b2, c2, and d2) of PBSt with typical extensor-type (type 2) and biphasic (type 3) activity profiles during resetting flexor and extensor deletions. In simulations, the traces represent histograms of average neuron activity in the motoneuron populations (Mn-F, Mn-E, Mn-PBSt, and Mn-RF). Shaded rectangles highlight the flexor, extensor, PBSt, and RF motoneuron population behavior during deletions.

In Fig. 5.12a1, before and after the flexor deletion, PBSt exhibits the extensor type activity profile (type 2) and RF shows the flexor type of activity (type 1). During the deletion, PBSt demonstrates sustained tonic activity similar to the extensor SmAB while RF becomes silent as the flexors (Sart and TA). Such PBSt and RF behavior was reproduced in our simulation shown in Fig. 5.13a2. In Fig. 5.12b1 before and after deletion, PBSt demonstrates an extensor-type activity profile (type 2). During the resetting extensor deletion, it becomes silent similar to extensors, which is reproduced in our simulation shown in Fig. 5.12b2. In Fig. 5.12c1, d2, before and after deletions, PBSt has a biphasic activity profile with a short flexor burst (type 3a) and becomes tonically active during the flexor deletion (Fig. 5.12c1) or silent during the extensor deletion (Fig. 5.12d1) (see also Table 5.1). Such behavior of the biphasic PBSt was reproduced in our simulations during flexor (Fig. 5.12c2) and extensor (Fig. 5.12d2) deletions.
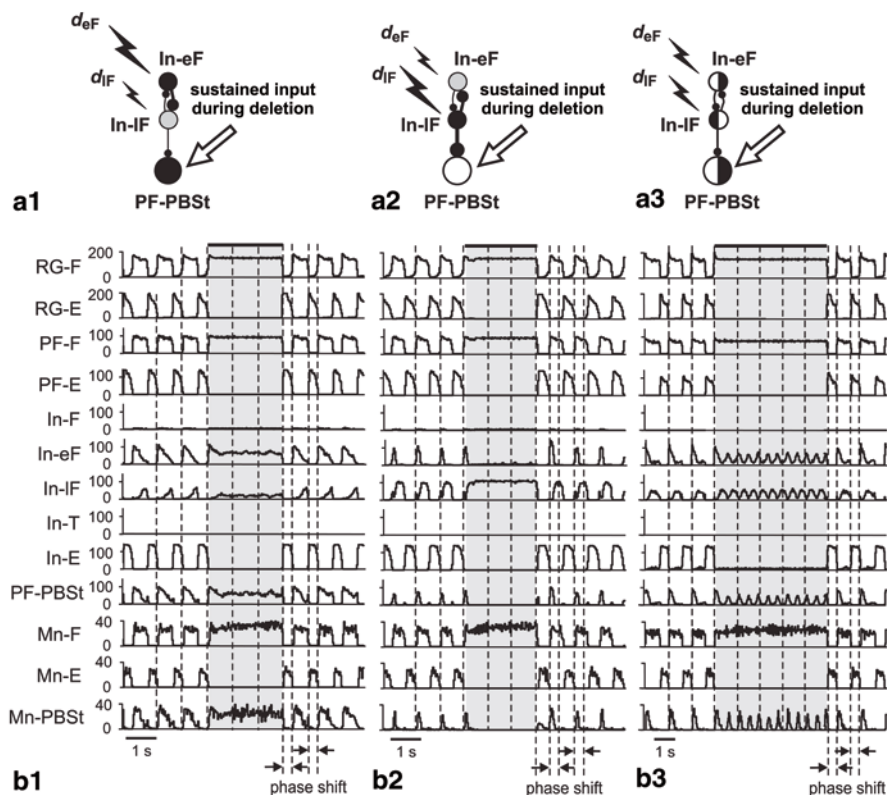
Fig. 5.11 Modeling of flexor-type PBSt behavior during resetting extensor deletions. **a1–a3** Circuits shaping the PF-PBSt population activity during deletions for: PBSt with a long flexor burst before and after the deletion (**a1**), a short flexor burst before and after the deletion (**a2**), and a flexor burst of about half of the flexor phase before and after the deletion (**a3**). Bolts of different sizes schematically show excitatory input drives of different strengths received by the In-eF and In-lF inhibitory populations, the larger the bolt size the stronger the input drive. Inhibition provided by a population is schematically represented by thickness of the corresponding output connection, the greater the strength of inhibition, the thicker the connection. Unfilled arrows illustrate sustained activation of the PF-PBSt populations during the deletions by the RG-F population (see Table 5.2). *Black circles* represent populations highly activated during deletions; *gray circles* illustrate a low level of activation in populations; unfilled circle indicates the inactive population; *half-filled circles* indicate phasic activity of populations. **b1–b3** Results of simulation of PBSt behavior during deletions shown in Fig. 5.5a–c. Simulated deletions were produced by a temporal decrease (by 50 %) of the MLR tonic excitatory drive to the RG-E population indicated by horizontal black bars at the top of traces. Each trace represents a histogram of average neuron activity in a particular population (spikes per neuron per second, bin = 30 ms). Two upper traces show activities of the RG-F and RG-E populations followed by activities of the PF-F and PF-E populations (third and fourth traces). Next five traces show activities of the hypothetical interneuron populations shaping the PF-PBSt population activity (see Figs. 5.6–5.9). The fourth trace from the bottom shows activity of the PF-PBSt population. Three lower traces show activities of the Mn-F, Mn-E, and Mn-PBSt populations, respectively. *Shaded rectangles* highlight behaviors of neuron populations during the deletions. An obvious phase shift of the post-deletion rhythm with respect to the pre-deletion rhythm (see arrows at the bottom of traces) indicates that the deletions are resetting
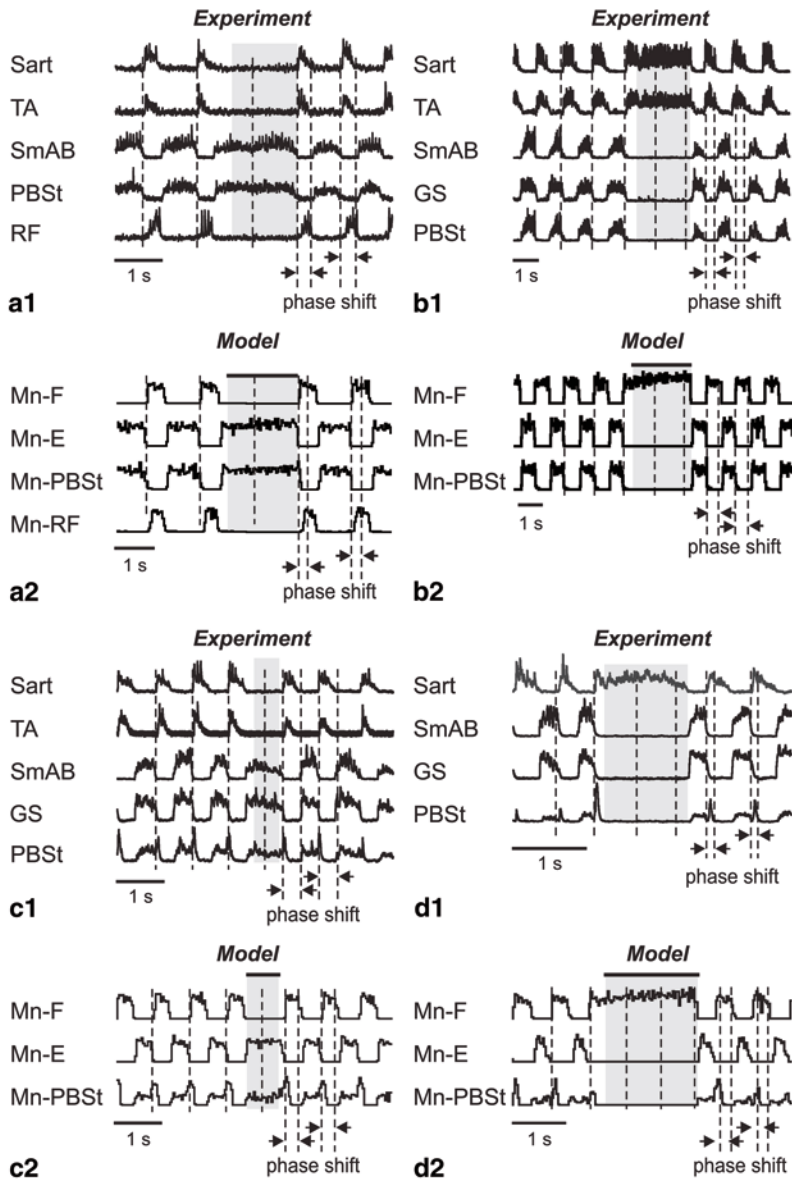
Fig. 5.12 Simulation of the extensor-type (type 2) and biphasic (type 3) PBSt and flexor-type (type 1) RF behavior during resetting deletions (see an obvious phase shift of the post-deletion rhythm with respect to the pre-deletion rhythm). Shaded rectangles highlight flexor, extensor, PBSt and RF behaviors during deletions. **a1, b1, c1, d1** Experimental recordings demonstrating the PBSt and RF (in **a1**) behavior during the extensor (**a1, c1**) and flexor (**b1, d1**) deletions. **a2, b2, c2, d2** Simulation of experimental results shown in **a1, b1, c1, d1.** The traces represent histograms of average neuronal activity in the Mn-F, Mn-E, Mn-PBSt, and Mn-RF (in **a2**) populations. Horizontal bars above the traces indicate temporal increase of the MLR drive to the RG- or RG-F populations (by 20 % in **a2**, **b2**, **c2** and by 10 % in **d2**). For values of input drives to the RG-E, RG-E, and hypothetical interneuron populations see Table 5.A3 in Appendix.
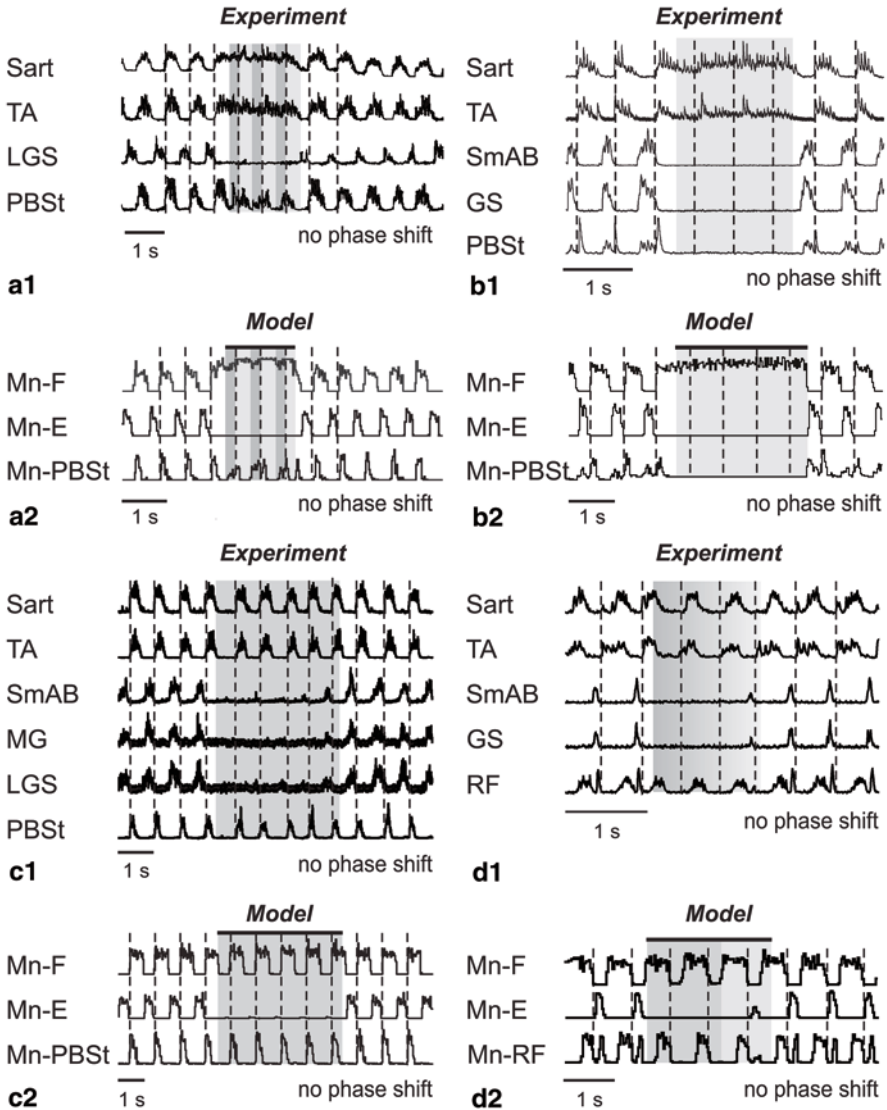
5.4.2.2 Non-Resetting Deletions

According to the two-level locomotor CPG organization, non-resetting extensor deletions could be caused by spontaneous perturbations at the PF level (Rybak et al. 2006a). In the model, this deletion type can be reproduced by a temporal change in the MLR drive to the corresponding PF population. In turn, the RG populations continue rhythmic activity and maintain the phase of oscillations during non-resetting deletions. The perturbation producing deletion affects the principal populations at the PF level, so that either PF-F or PF-E becomes silent, while the opposite principal population (PF-E or PF-F) switches to sustained activity or remains rhythmic (PF-F) (see Table 5.2). Thus, during non-resetting deletions, behaviors of the interneuron populations shaping activity profiles of the PF-PBSt and PF-RF populations (and hence Mn-PBSt and Mn-RF) are influenced by two factors: continuing rhythmic inputs from the RG populations and either sustained or lost inputs from the PF level.

Figure 5.13 shows our modelling of PBSt and RF typical behaviors during non-resetting extensor deletions with tonic (Fig. 5.13a1, a2, b1, b2) and rhythmic (Fig. 5.13c1, c2, d1, d2) activity in flexors. Upper panels (a1, b1, c1, and d1) show the experimental recordings and the lower panels (a2, b2, c2, and d2) demonstrate our simulation results. Shaded rectangles highlight flexor, extensor, PBSt and RF behavior during deletions.

Figure 5.13a1, b1 shows the behavior of flexor- and biphasic (with a short flexor burst, type 3a) types of PBSt during non-resetting deletions of extensor activity (SmAB, MG, LGS, and LG) when flexors (TA and Sart) switched to sustained activity. In the corresponding simulations shown in Fig. 5.13a2, b2, the non-resetting extensor deletions were produced by temporal increase of the MLR drive to the PF-F population (Rybak et al. 2006a). In Fig. 5.13a1, PBSt is active during most of the flexor phase (type 1b) before and after the deletion and demonstrates activity in both flexor and extensor expected phases during deletion. This resembles PBSt behavior during the non-resetting deletion shown in Fig. 5.5d1 and is typical for PBSt having the type 1b activity pattern (see Table 5.1). The corresponding simulation is shown in Fig. 5.13a2. In Fig. 5.13b1, the PBSt activity pattern is biphasic with a short flexor burst (type 3a) before and after the deletion. During a non-resetting extensor deletion, PBSt becomes silent as extensors (SmAB and GS) which is reproduced in our simulation shown in Fig. 5.13b1.

Figure 5.13c1, c2, d1, d2 shows two examples (panels c1 and d1) of non-resetting deletions of extensor activity (SmAB, MG, LGS, and LG) while flexors (TA and Sart) remain rhythmically active and the corresponding simulations (panels c2 and d2). In simulations, the non-resetting deletions of extensor activity were produced by temporal suppression of the PF-E population activity by application of an additional inhibitory drive to this population, while the PF-F population continued receiving the rhythmic input from the RG-F population and transferring it to the Mn-F population (Rybak et al. 2006a). In Fig. 5.13c1, PBSt is active in the beginning of the flexor phase (type 1) before and after the deletion and continues rhythmic activity during extensor deletion together with the flexors (Sart and TA). This is

Fig. 5.13 Modeling of PBSt with flexor (type 1) and biphasic (type 2) behavior during non-resetting extensor deletions with tonically active or rhythmic flexors. Shaded rectangles highlight flexor, extensor, PBSt and RF activity during deletions. **a1** and **b1** Experimental recordings demonstrating flexor-type PBSt activity during non-resetting deletions with tonically active flexors (Sart and TA). **a2, b2** Simulation of experimental results shown in **a1** and **b1**. *Horizontal bars* in **a2** and **b2** above the traces indicate temporal increase of the MLR drive to the PF-F population by 30 % (both in **a2** and **b2**). **c1, d1:** Experimental recordings demonstrating biphasic PBSt (**c1**, modified from Lafreniere-Roula and McCrea 2005) or RF (**d1**) behavior during non-resetting extensor deletions with rhythmically active flexors (Sart and TA). **a2, b2** Simulation of experimental results shown in **c1** and **d1**. Horizontal bars above the traces indicate temporal suppression of the PF-E population activity by an inhibitory drive ($d_{inh} = 0.7$ in both **a2** and **b2**). In **b2**, changing level of shading schematically shows reduction of the additional inhibitory drive to the PF-E population by 70 %. See text for details. The traces in **a2, b2, c2**, and **d2** represent histograms of average neuronal activity in the Mn-F, Mn-E and Mn-PBSt or Mn-RF populations. For values of input drives to the RG-E, RG-E, and hypothetical interneuron populations see Table 5.A3 in Appendix

reproduced in our simulation shown in Fig. 5.13c2. Figure 5.13d1 shows the behavior of the biphasic RF during the non-resetting extensor deletion while flexors (Sart and TA) continue rhythmic activity. Interestingly, similar to the behavior of the biphasic RF during non-resetting deletions with tonic flexor activity (Fig. 5.5d1), in the experimental recording shown in Fig. 5.13d1, RF loses its extensor component during the deletion. The corresponding simulation reproducing the biphasic RF behavior during the extensor deletion with rhythmically active flexors is shown in Fig. 5.13d2. Similar to the experimental records, the Mn-RF population during the deletion maintains rhythmic activity but loses the extensor component of its activity profile. Our simulation shows a striking similarity to the experimental recordings including the low-amplitude extensor and RF bursts by the end of the deletion.

5.5   Discussion

The bipartite half-center organization of the locomotor CPG originally proposed by T. Graham Brown (1914) and expanded by Lundberg, Jankowska and their colleagues (Jankowska 1967a, b; Lundberg 1981; Stuart and Hultborn 2008) could not explain the complex activity patterns of two-joint muscles and the corresponding motoneurons recorded during real or fictive locomotion. This motivated researchers to search for alternative concepts for CPG organization. For example, Grillner (1981) has suggested a Unit Burst Generators (UBGs) model consisting of multiple coupled oscillators each of which operates at each joint. The UBG architecture is much more flexible and functionally richer than the original half-center CPG architecture. However, no UBG-based CPG computational model has been developed so far that could reproduce the complex patterns of bifunctional motoneurons. In contrast, Perret and colleagues (Perret and Cabelguen 1980; Perret 1983; Orsal et al. 1986; Perret et al. 1988) have proposed a solution for this problem in the framework of the bipartite locomotor CPG. They suggested that the bifunctional motoneurons (PBSt and RF) receive excitatory and inhibitory inputs from both flexor and extensor CPG half-centers and that special circuit organization within the CPG can shape the activity profiles of bifunctional motoneurons. This suggestion was used as a basis for our model development.

Our approach was based on a recently proposed concept of a two-level organization of the spinal locomotor CPG (Rybak et al. 2006a, b; McCrea and Rybak 2007, 2008). According to this concept, a bipartite half-center RG controls operation of PF networks that in turn coordinate rhythmic excitation and inhibition of multiple synergist motoneuron pools during locomotion. The proposed two-level CPG architecture has a number of advantages including the possibility for independent control of locomotor rhythm and phase durations at the RG level and control of patterns of motoneuron activations at the PF level. The two-level CPG organization proposed explanations for many experimental findings observed during fictive locomotion, including the specific alteration of activity of flexor and extensor motoneurons during afferent stimulations (Rybak et al. 2006b; McCrea and Rybak 2007; Shevtsova

2015) and their behavior during spontaneous deletions of motoneuron activity occurring with and without resetting of the locomotor cycle (Rybak et al. 2006a; McCrea and Rybak 2008; Shevtsova 2015). This two-level organization had been implemented in the reduced computational model of the CPG (Fig. 5.3) that could generate a realistic locomotor rhythm with alternating activity profiles of flexor and extensor motoneuron pools and reproduce various changes of these profiles under different conditions, such as afferent stimulations and deletions (Rybak et al. 2006a, b; Shevtsova 2015). However, this reduced model considered only two antagonist motoneuron populations (flexors and extensors) and did not include bifunctional motoneuron pools which are known to express more complicated firing patterns during both fictive and real locomotion. The major objective of this study was to extend the basic two-level CPG model by suggesting a special organization of the PF circuits, while keeping the bipartite organization of the RG. To this end, the proposed extended model reproduces the full repertoire of PBSt and RF motoneuron activity patterns recorded during fictive locomotion as well as all changes of these patterns observed during various deletions.

5.5.1 The Extended CPG Model Circuitry

The idea that excitatory and inhibitory inputs from both extensor and flexor parts of the bipartite locomotor rhythm generator provide shaping of PBSt and RF motoneuron activity patterns suggested by Perret and colleagues (Perret and Cabelguen 1980; Perret 1983; Orsal et al. 1986; Perret et al. 1988) has not been implemented previously in a computational model. Moreover, the Perret schematic, through incorporating some additional neuronal networks shaping PBSt and RF motoneuron activities, can provide explanation for only the biphasic PBSt and RF patterns and cannot explain the variety of PBSt and RF activity profiles observed during fictive locomotion and the specific behaviors of PBSt and RF motoneuron populations during spontaneous deletions. Perret and colleagues (Perret et al. 1988) believed that the variability of PBSt and RF activity patterns is a result of interactions between the central locomotor drive and afferent influences. However, the analysis of fictive locomotion experiments in decerebrate cats (Markin et al. 2012) has shown that the full repertoire of non-trivial activity profiles of PBSt and RF can be generated in the absence of sensory feedback and hence may represent an inherent property of the locomotor CPG. By analyzing the PBSt and RF activity patterns we proposed a hypothetical network of interneuron populations incorporated in the pattern formation (PF) level of the two-level spinal CPG that can provide for the full repertoire of the PBSt and RF motoneuron activity profiles and explain their behaviors during deletions.

The key elements of the proposed network are (1) the principal neuron populations (PF-PBSt and PF-RF, see Fig. 5.8) that directly control activation of the PBSt and RF motoneuron pools, and (2) additional interneuron populations (In-E, In-T, In-F, In-lF, In-eF, In-eE, and, In-lE, see Fig. 5.8) that shape the activity profiles of the PF-PBSt and PF-RF populations during the flexor and extensor phases.

In the model, the activation of these interneuron populations (or the drives they receive from MLR) explicitly defines the activity profiles expressed during particular fictive locomotion experiment (from the repertoire of possible profiles). We suggest that these are the populations that during real locomotion receive excitatory input from sensory afferents and/or descending signals which, therefore, can select and shape the appropriate activity profiles of PBSt and RF motoneuron pools to adjust their activity to gait and speed of locomotion, and particular locomotor conditions.

It appears that activity of PB and RF (and other two-joint muscles) is tightly regulated by descending and afferent signals, so that the phasing and magnitude of their activity corresponds precisely to the mechanical demands. During skilled locomotor behaviors (walking, running, cycling (Wells and Evans 1987; Prilutsky et al. 1998a; Prilutsky and Gregor 2000) and other skilled non-rhythmic behaviors (load lifting or isometric exertion of external forces by the leg (Wells and Evans 1987; Prilutsky et al. 1998b), two-joint muscles typically exhibit their highest activity when they can simultaneously contribute to the extensor or flexor actions of all synergists at both joints the two-joint muscle crosses; the two-joint muscles are typically inhibited, when their anatomical antagonists at both joints produce the actions opposite to the ones of the two-joint muscle (Prilutsky 2000). During overground normal level and slope walking different bursts of PB and RF can be associated with actions of the corresponding flexor and extensor muscles at the knee and hip joints. For example, electromyogram (EMG) bursts of the PB muscle (knee flexor and hip extensor) are closely associated with the knee flexor-hip extensor combination of the resultant muscle moments in early swing and late swing-early stance phases of level and slope walking (Carlson-Kuhta et al. 1998; Smith et al. 1998a; Gregor et al. 2006). Similarly, the stance related EMG burst of the RF muscle (knee extensor-hip flexor) can be associated with the knee extensor-hip flexor combination of the resultant muscle moments (Carlson-Kuhta et al. 1998; Smith et al. 1998a; Gregor et al. 2006). Such organization of neural control of two-joint muscles appears to minimize total muscle stress, effort, fatigue and other related physiological variables as demonstrated by similarity between recorded EMG patterns of two-joint muscles and the muscle activity or muscle force patterns computed by minimizing the above cost functions in a musculoskeletal model during the same motor task (Anderson and Pandy 2001; Prilutsky and Zatsiorsky 2002).

5.6   Conclusion

Construction of a CPG model that would be able to realistically reproduce the behavior of the PBSt and RF during fictive locomotion required a comprehensive analysis of firing profiles of these motoneuron pools during fictive locomotion (Markin et al. 2012) and their behaviors during spontaneous deletions. This analysis allowed us to construct an extended model of the locomotor CPG by incorporating additional neuronal network to shape PBSt and RF activity profiles. To our knowledge this is the first computational model reproducing behavior of PBSt and RF during locomotion.

We have demonstrated that a two-level locomotor CPG with the bipartite half-center rhythm generator and special organization of neural circuits at the pattern formation level can generate complex activity patterns of bifunctional motoneurons, such as PBSt and RF. The proposed CPG model reproduces the full repertoire of PBSt and RF activity patterns recorded during fictive locomotion. The model also suggests explanations for the observed variability of PBSt and RF activity and may predict their behavior under different conditions. We hypothesize that sensory inputs to selected interneuron populations within the pattern formation level of the CPG provide a mechanism for the proprioceptive control of the activity of bifunctional motoneurons during real locomotion.

Appendix

All neurons were modelled in the Hodgkin-Huxley style. Motoneurons had two compartments: soma and dendrite and were described based on the previous models (Booth et al. 1997; Rybak et al. 2006a). The membrane potentials of motoneuron soma ($V_{(S)}$) and dendrite ($V_{(D)}$) obey the following differential equations:

$$C \times \frac{dV_{(S)}}{dt} = -I_{Na(S)} - I_{K(S)} - I_{A(S)} - I_{CaN(S)} - I_{K,Ca(S)} - I_{L(S)} - I_{C(S)}$$

$$C \times \frac{dV_{(D)}}{dt} = -I_{NaP(D)} - I_{CaN(D)} - I_{CaL(D)} - I_{K,Ca(D)} - I_{L(D)} - I_{C(D)} - I_{SynE} - I_{SynI}$$

$$\text{(5.A1)}$$

where C is the membrane capacitance and t is time ($C = 1$ μF/cm^2), subscripts S and D indicate the soma or dendrite compartments, respectively.

The dendrite-soma coupling currents (with conductance g_C) for soma $I_{C(S)}$ and dendrite $I_{C(D)}$ are described as follows:

$$I_{C(S)} = \frac{g_C}{p} \times (V_{(S)} - V_{(D)});$$

$$I_{C(D)} = \frac{g_C}{1-p} \times (V_{(D)} - V_{(S)}), \qquad \text{(5.A2)}$$

where p is the parameter defining the ratio of somatic surface area to total surface area ($p = 0.1$); $g_C = 0.1$ mS/cm^2.

The following currents (with the corresponding maximal channel conductances) are included into motoneuron soma compartments (Booth et al. 1997; Rybak et al. 2006a): fast sodium, I_{Na} (maximal conductance $\bar{g}_{Na} = 120$ mS/cm^2); persistent sodium, I_K ($=\bar{g}_{NaP}$ 100 mS/cm^2); calcium-N, I_{CaN} ($\bar{g}_{CaN} = 14$ mS/cm^2); calcium-dependent potassium, $I_{K, Ca}$ ($\bar{g}_{CaL} = 2$ mS/cm^2), and leakage, I_L ($g_L = 0.51$ mS/cm^2) currents. In addition, based on evidence of the presence of the transient (rapidly inactivating) potassium current in the spinal cord interneurons and motoneurons (Safronov and Vogel 1995) this current has been also included in our motoneuron models (I_A with maximal conductance $\bar{g}_A = 200 \pm 40$ mS/cm^2). The following currents (with the corresponding maximal channel conductances) are included into motoneuron dendritic compartment: persistent sodium, I_{NaP} ($\bar{g}_{NaP} = 0.1$ mS/cm^2); calcium-N, I_{CaN} ($\bar{g}_{CaN} = 0.3$ mS/cm^2); calcium-L (I_{CaL}, $\bar{g}_{CaL} = 0.33$ mS/cm^2), calcium-dependent potassium, $I_{K, Ca}$ ($\bar{g}_{K,Ca} = 0.8$ mS/cm^2), and leakage, I_L ($g_L = 0.51$ mS/cm^2) currents.

Interneurons are simulated as single-compartment models. The neurons within the RG-F, RG-E, PF-F, PF-E, In-eF, and In-eE populations contain fast sodium, I_{Na}; persistent sodium, I_{NaP}; delayed-rectifier potassium, I_K; and leakage, I_L currents:

$$C \times \frac{dV}{dt} = -I_{Na} - I_K - I_L - I_{SynE} - I_{SynI} \qquad (5.A3)$$

The maximal channel conductances for neurons in theses populations are as follows: $g_L = 0.51$ mS/cm^2; $\bar{g}_{Na} = 150$ mS/cm^2 in RG-F and RG-E neurons and 120 mS/cm^2 in the PF-F, PF-E, In-eF, and In-eE populations; $\bar{g}_{NaP} = 1.25$ mS/cm^2 in RG-F, RG-E, In-eF, and In-eF neurons and 0.1 mS/cm^2 in the PF-F and PF-E populations; $\bar{g}_K = 5$ mS/cm^2 in the RG-F and RG-E populations and 10 mS/cm^2 in the PF-F, PF-E, In-eE, and In-eF populations.

For simplicity, all other interneurons contain only minimal set of ionic currents:

$$C \times \frac{dV}{dt} = -I_{Na} - I_K - I_L - I_{SynE} - I_{SynI} \qquad (5.A4)$$

with the following maximal conductances: $\bar{g}_{Na} = 120$ mS/cm^2; $\bar{g}_K = 10$ mS/cm^2; $g_L = 0.51$ mS/cm^2.

The ionic currents included into the modelled neurons are described as follows:

$$
\begin{aligned}
I_{Na} &= \bar{g}_{Na} \times m_{Na}^3 \times h_{Na} \times (V - E_{Na}); \\
I_{NaP} &= \bar{g}_{NaP} \times m_{NaP} \times h_{NaP} \times (V - E_{Na}); \\
I_K &= \bar{g}_K \times m_K^4 \times (V - E_K); \\
I_A &= \bar{g}_A \times (0.6 \times m_{A1}^4 \times h_{A1} + 0.4 \times m_{A2}^4 \times h_{A2}) \times (V - E_K); \\
I_{CaN} &= \bar{g}_{CaN} \times m_{CaN}^2 \times h_{CaN} \times (V - E_{Ca}); \\
I_{CaL} &= \bar{g}_{CaL} \times m_{CaL} \times (V - E_{Ca}); \\
I_{K,Ca} &= \bar{g}_{K,Ca} \times m_{K,Ca} \times (V - E_K); \\
I_L &= g_L \times (V - E_L),
\end{aligned}
\qquad (5.A5)
$$

where V is the membrane potential of the corresponding neuron compartment (soma, $V_{(S)}$, or dendrite, $V_{(D)}$) in two-compartment models, or the neuron membrane potential V in one-compartment models; E_{Na}, E_K, E_{Ca}, and E_L are the reversal potentials for sodium, potassium, calcium, and leakage current respectively; variables m and h with indexes indicating ionic currents represent, respectively, the activation and inactivation variables of the corresponding ionic channels.

The reversal potential values in the model are as follows: $E_{Na}=55$ mV; $E_K=-80$ mV; $E_{Ca}=80$ mV; $E_L=-64\pm0.64$ mV in RG-F and RG-E neurons, $E_L=-65\pm0.325$ mV in Inrg-F and Inrg-E interneurons and motoneurons, and $E_L=-68\pm0.34$ mV in all other neurons.

Activation m and inactivation h of voltage-dependent ionic channels (e.g., Na, NaP, K, A, CaN, CaL) are described by the following differential equations:

$$\tau_{mi}(V)\times\frac{d}{dt}m_i = m_{\infty i}(V)-m_i;$$
$$\tau_{hi}(V)\times\frac{d}{dt}h_i = h_{\infty i}(V)-h, \tag{5.A6}$$

where i identifies the name of the channel, $m_{\infty i}(V)$ and $h_{\infty i}(V)$ represent the voltage-dependent steady-state activation and inactivation respectively, and $\tau_{mi}(V)$ and $\tau_{hi}(V)$ define the corresponding time constants (see their descriptions in Table 5.A1). Activation of the sodium channels is considered to be instantaneous ($\tau_{mNa}=\tau_{mNaP}=0$, see (Booth et al. 1997; Butera et al. 1999)).

Activation of the Ca^{2+}-dependent potassium channels is also considered instantaneous and described as follows (Booth et al. 1997):

$$m_{K,Ca} = \frac{Ca}{Ca+K_d}, \tag{5.A7}$$

where Ca is the Ca^{2+} concentration within the corresponding compartment of motoneuron, and K_d defines the half-saturation level of this conductance.

The kinetics of intracellular Ca^{2+} concentration (Ca, described separately for each compartment) is modelled according to the following equation (Booth et al. 1997):

$$\frac{d}{dt}Ca = f\times(-\alpha\times I_{Ca}-k_{Ca}\times Ca), \tag{5.A8}$$

where f defines the percent of free to total Ca^{2+}; α converts the total Ca^{2+} current, I_{Ca}, to Ca^{2+} concentration; k_{Ca} represents the Ca^{2+} removal rate.

The synaptic excitatory (I_{synE} with conductance g_{synE} and reversal potential $E_{SynE}=-10$ mV) and inhibitory (I_{synI} with conductance g_{synI} and reversal potential $E_{SynI}=-70$ mV) currents are described as follows:

$$I_{SynE} = g_{SynE}\times(V-E_{SynE});$$
$$I_{SynI} = g_{SynI}\times(V-E_{SynI}). \tag{5.A9}$$

Table 5.A1 Steady state activation and inactivation variables and time constants for voltage-dependent ionic channels

Ionic channels	$m_\infty(V)$, V is in mV $h_\infty(V)$, V is in mV	$\tau_m(V)$, ms $\tau_h(V)$, ms
Na	$m_{\infty Na} = (1+\exp(-(V+35)/7.8))^{-1}$	$\tau_{mNa} = 0$
	$h_{\infty Na} = (1+\exp((V+55)/7))^{-1}$	$\tau_{hNa} = 30/(\exp((V+50)/15)+$ $\exp(-(V+50)/16))$
NaP	$m_{\infty NaP} = (1+\exp(-(V+47.1)/3.1))^{-1}$	$\tau_{mNaP} = 0$
	$h_{\infty NaP} = (1+\exp((V+59)/8))^{-1}$	$\tau_{hNaP} = 800/\cosh((V+59)/16)$
K	$m_{\infty K} = (1+\exp(-(V+28)/15))^{-1}$	$\tau_{mK} = 7/(\exp((V+40)/40)+$ $\exp(-(V+40)/50))$
	$h_K = 1$	N/A
A	$m_{\infty A1} = (1+\exp(-(V+60)/8.5))^{-1}$	$\tau_{mA1} = 1/(\exp((V+35.82)/19.69)+$ $\exp(-(V+79.69)/12.7)+0.37)$
	$h_{\infty A1} = (1+\exp((V+78)/6))^{-1}$	$\tau_{hA1} = 1/(1+\exp((V+46.05)/5)+$ $\exp(-(V+238.4)/37.45))$ If $V<-63$, otherwise $\tau_{hA1}=19.0$
	$m_{\infty A2} = (1+\exp(-(V+36)/20))^{-1}$	$\tau_{mA2} = 1/(\exp((V+35.82)/19.69)+$ $\exp(-(V+79.69)/12.7)+0.37)$
	$h_{\infty A2} = (1+\exp((V+78)/6))^{-1}$	$\tau_{hA2} = 1/(1+\exp((V+46.05)/5)+$ $\exp(-(V+238.4)/37.45))$ If $V<-73$, otherwise $\tau_{hA2}=60.0$
CaN	$m_{\infty CaN} = (1+\exp(-(V+30)/5))^{-1}$	$\tau_{mCaN} = 4$
	$h_{\infty CaN} = (1+\exp((V+45)/5))^{-1}$	$\tau_{hCaN} = 40$
CaL	$m_{\infty CaL} = (1+\exp(-(V+40)/7))^{-1}$	$\tau_{mCaL} = 40$
	$h_{CaL} = 1$	N/A

All expressions and parameters, except those for the NaP and potassium A channels, are taken from (Booth et al. 1997). The expressions for the NaP channel are from (Rybak et al. 2003). The expressions for potassium A channel are from (Huguenard and McCormick 1991; Huguenard and McCormick 1992).

The excitatory (g_{SynE}) and inhibitory synaptic (g_{SynI}) conductances are equal to zero at rest and may be activated (opened) by the excitatory or inhibitory inputs to neuron i respectively:

$$g_{SynEi}(t) = \overline{g}_E \times \sum_j \sum_{t_{kj}<t} S\{w_{ji}\} \times \exp(-(t-t_{kj})/\tau_{SynE}) + \overline{g}_{Ed} \times \sum_m S\{w_{dmi}\} \times d_{mi};$$

$$g_{SynIi}(t) = \overline{g}_I \times \sum_j \sum_{t_{kj}<t} S\{-w_{ij}\} \times \exp(-(t-t_{kj})/\tau_{SynI}) + \overline{g}_{Id} \times \sum_m S\{-w_{dmi}\} \times d_{mi},$$

$$(5.A10)$$

Table 5.A2 Weights of synaptic connections between populations in the network

Target population	Source population (weight of synaptic input to one neuron)
RG-E	RG-E (0.00125); RG-F (0.00125); Inrg-E (−0.01125)
RG-F	RG-E (0.00125); RG-F (0.00125); Inrg-F (−0.01125)
Inrg-E	RG-F (0.03)
Inrg-F	RG-E (0.03)
PF-E	RG-E (0.005); Inrg-E (−0.0035); Inpf-E (−0.04)
PF-F	RG-F (0.005); Inrg-F (−0.0035); Inpf-F (−0.04)
Inpf-E	PF-F (0.025)
Inpf-F	PF-E (0.025)
PF-PBSt	RG-E (0.005); RG-F (0.005); In-E (−0.02); In-eF (−0.02)
PF-RF	PF-E (0.015); RG-F (0.005); In-eE (−0.05); In-eF (−0.02)
In-E	PF-E (0.05); Inrg-F (−0.02): In-T (−0.0125)
In-F	PF-F (0.05); Inrg-E (−0.02):
In-eF	Inrg-E (−0.02); In-lF(−0.0125)
In-lF	PF-F (0.005); Inrg-E (−0.0125); In-eF (−0.0125)
In-eE	PF-E (0.005); Inpf-F (−0.02)
In-lE	InrgF (−0.0125); In-T (−0.0125)
Ia-E	PF-E (0.0275); Ia-E (−0.02); R-E (−0.02)
Ia-F	PF-F (0.0275); Ia-F (−0.02); R-F (−0.02)
R-E	Mn-E (0.015); R-F (−0.015)
R-F	Mn-F (0.0015); R-E (−0.015)
R-PBSt	Mn-PBSt (0.015)
R-RF	Mn-RF (0.015)
Mn-E	PF-E (0.05); Ia-F (−0.04); R-E (−0.0025)
Mn-F	PF-F (0.05); Ia-E (−0.04); R-F (−0.0025)
Mn-PBSt	PF-PBSt (0.05); R-PBSt (−0.0025)
Mn-RF	PF-RF (0.05); R-RF (−0.0255)

Values in brackets represent relative weights of synaptic inputs from the corresponding source populations (w_{ji} or $-w_{ji}$).

where the function $S\{x\}=x$, if $x \geq 0$, and 0 if $x<0$. According to equation (5.A10), the excitatory and inhibitory synaptic conductances have two terms: the first term describes the effects of inputs from other neurons in the network (excitatory and inhibitory respectively), and the second one describes effects of inputs from external drives d_{mi} (see also Rybak et al. 1997). Each spike arriving to neuron i from neuron j at time t_{kj} increases the excitatory synaptic conductance by $\bar{g}_E \times w_{ji}$ if the synaptic weight $w_{ji}>0$, or increases the inhibitory synaptic conductance by $-\bar{g}_I \times w_{ji}$ if the synaptic weight $w_{ji}<0$. $\bar{g}_E=0.05$ mS/cm² and $\bar{g}_I=0.05$ mS/cm² are the parameters defining an increase in the excitatory or inhibitory synaptic conductance, respectively, produced by one arriving spike at $|w_{ji}|=1$. $\tau_{SynE}=5$ ms and $\tau_{SynE}=15$ ms are the decay time constants for the excitatory and inhibitory conductances respectively. In the second terms of equations (5.A10), $\bar{g}_{Ed}=\bar{g}_{Id}=1$ mS/cm² is the parameter defining the increase in the excitatory synaptic conductance, produced by external input drive $d_{mi}=1$ with a synaptic weight of $|w_{dmi}|=1$. All synaptic weights used in the model can be found in Table 5.A2. The values of input drives used in particular simulation are shown in Table 5.A3.

Table 5.A3 Values of input drives in simulations

Figure No	d_{RG-E}	d_{RG-F}	d_E	d_T	d_F	d_{eF}	d_{IF}	d_{eE}	d_{IE}
9B1	0.17	0.18	0.25	0	0	0.18	0.17	N/A	N/A
9B2	0.17	0.18	0	0.3	0.3	N/A	N/A	N/A	N/A
9B3	0.17	0.18	0.2	0.1	0	0.18	0.22	N/A	N/A
9B4	0.17	0.18	N/A	0.3	N/A	0.2	0.2	0.22	0.25
9B5	0.17	0.18	N/A	0	N/A	0.2	0.2	0.22	0.25
10A2	0.175	0.17	0.25	0	0	0.17	0.22	0.2	0
10B2	0.18	0.19	0.25	0	0	0.2	0.28	0.2	0
10C2	0.185	0.175	0	0.25	0.25	0.17	0.22	0.2	0
10D2	0.175	0.17	0.1	0	0	0.17	0.22	0.2	0
11B1	0.175	0.195	0.25	0	0	0.18	0.185	N/A	N/A
11B2	0.18	0.19	0.25	0	0	0.17	0.23	N/A	N/A
11B3	0.16	0.18	0.25	0	0	0.18	0.16	N/A	N/A
12A2	0.165	0.15	0	0.25	0.25	0.16	0.23	0.2	0
12B2	0.15	0.15	0	0.25	0.25	0.18	0.22	N/A	N/A
12C2	0.18	0.19	0.1	0	0	0.18	0.2	N/A	N/A
12D2	0.18	0.205	0.1	0	0	0.18	0.17	N/A	N/A
13A2	0.17	0.21	0.12	0	0	0.16	0.21	0.25	0.1
13B2	0.18	0.205	0.09	0	0	0.18	0.17	0.22	0
13C2	0.16	0.175	0.25	0	0	0.2	0.17	N/A	N/A
13C2	0.16	0.175	N/A	0.1	N/A	0.2	0.2	0.22	0.25

Values of MLR drives to the PF-E and PF-F populations in all simulations were $d_{PF-E} = d_{PF-F} = 0.1$; to the PF-PBSt and RF populations, $d_{PF-E} = d_{PF-F} = 0$.

References

Anderson FC, Pandy MG (2001) Static and dynamic optimization solutions for gait are practically equivalent. J Biomech 34:153–161

Booth V, Rinzel J, Kiehn O (1997) Compartmental model of vertebrate motoneurons for Ca2+ -dependent spiking and plateau potentials under pharmacological treatment. J Neurophysiol 78:3371–3385

Brown TG (1914) On the nature of the fundamental activity of the nervous centres; together with an analysis of the conditioning of rhythmic activity in progression, and a theory of the evolution of function in the nervous system. J Physiol 48:18–46

Butera RJ, Jr., Rinzel J, Smith JC (1999) Models of respiratory rhythm generation in the pre-Botzinger complex. I. Bursting pacemaker neurons. J Neurophysiol 82:382–397

Carlson-Kuhta P, Trank TV, Smith JL (1998) Forms of forward quadrupedal locomotion. II. A comparison of posture, hindlimb kinematics, and motor patterns for upslope and level walking. J Neurophysiol 79:1687–1701

Gregor RJ, Smith DW, Prilutsky BI (2006) Mechanics of slope walking in the cat: quantification of muscle load, length change, and ankle extensor EMG patterns. J Neurophysiol 95:1397–1409

Grillner S (1981) Control of locomotion in bipeds, tetrapods, and fish. In: Brooks V (ed) Handbook of physiology. section I. The nervous system, Vol II. American Physiological Society, Bethesda, pp 1179–236

Grillner S, Zangger P (1979) On the central generation of locomotion in the low spinal cat. Exp Brain Res 34:241–261

Guertin P, Angel MJ, Perreault MC, McCrea DA (1995) Ankle extensor group I afferents excite extensors throughout the hindlimb during fictive locomotion in the cat. J Physiol 487(Pt 1):197–209

Halbertsma JM (1983) The stride cycle of the cat: the modelling of locomotion by computerized analysis of automatic recordings. Acta Physiol Scand Suppl 521:1–75

Hamade K, Shevtsova NA, Markin SN, Chakrabarty S, McCrea DA, Rybak IA (2008) How a bipartite CPG can control the activity of bifunctional motoneurons: a modeling study with insights from deletions during fictive locomotion. In 2008 Neuroscience Meeting Planner. Society for Neuroscience. Abstract 925.4. Washington, DC.

Huguenard JR, McCormick DA (1991) Vclamp and Cclamp. A computational simulation of single thalamic relay and cortical pyramidal neurons. Neural simulation instruction manual. Stanford University, Stanford

Huguenard JR, McCormick DA (1992) Simulation of the currents involved in rhythmic oscillations in thalamic relay neurons. J Neurophysiol 68:1373–1383

Jankowska E, Jukes MG, Lund S, Lundberg A (1967a) The effect of DOPA on the spinal cord. 5. Reciprocal organization of pathways transmitting excitatory action to alpha motoneurones of flexors and extensors. Acta Physiol Scand 70:369–388

Jankowska E, Jukes MG, Lund S, Lundberg A (1967b) The effect of DOPA on the spinal cord. 6. Half-centre organization of interneurones transmitting effects from the flexor reflex afferents. Acta Physiol Scand 70:389–402

Lafreniere-Roula M, McCrea DA (2005) Deletions of rhythmic motoneuron activity during fictive locomotion and scratch provide clues to the organization of the mammalian central pattern generator. J Neurophysiol 94:1120–1132

Lundberg A (1981) Half-centres revisited. In: Szentagothai J, Palkovits M, Hamori J (eds) Regulatory functions of the CNS. Motion and organization principles. Pergamon Akadem Kiado, Budapest, pp 155–167

MacGregor RI (1987) Neural and brain modelling. Academic Press, New York

Markin SN, Lemay MA, Prilutsky BI, Rybak IA (2012) Motoneuronal and muscle synergies involved in cat hindlimb control during fictive and real locomotion: a comparison study. J Neurophysiol 107:2057–2071

McCrea DA, Chakrabarty S (2007) Activity patterns in bifunctional PBSt motoneuron pools during fictive locomotion in decerebrate cats: clues to CPG organization. In 2007 Neuroscience Meeting Planner. Society for Neuroscience. Abstract 925.3. Washington, DC.

McCrea DA, Rybak IA (2007) Modeling the mammalian locomotor CPG: insights from mistakes and perturbations. Prog Brain Res 165:235–253

McCrea DA, Rybak IA (2008) Organization of mammalian locomotor rhythm and pattern generation. Brain Res Rev 57:134–146

Orsal D, Perret C, Cabelguen JM (1986) Evidence of rhythmic inhibitory synaptic influences in hindlimb motoneurons during fictive locomotion in the thalamic cat. Exp Brain Res 64:217–224

Perret C (1983) Centrally generated pattern of motoneuron activity during locomotion in the cat. Symp Soc Exp Biol 37:405–422

Perret C, Cabelguen JM (1980) Main characteristics of the hindlimb locomotor cycle in the decorticate cat with special reference to bifunctional muscles. Brain Res 187:333–352

Perret C, Cabelguen JM, Orsal D (1988) Analysis of the pattern of activity in "knee flexor" motoneurons during locomotion in cat. In: Gurfinkel VS, Ioffe ME, Massim J (eds) Stance and motion: facts and concepts. Plenum Press, New York, pp 133–141

Pratt CA, Buford JA, Smith JL (1996) Adaptive control for backward quadrupedal walking V. Mutable activation of bifunctional thigh muscles. J Neurophysiol 75:832–842

Prilutsky BI (2000) Coordination of two- and one-joint muscles: functional consequences and implications for motor control. Motor Control 4:1–44

Prilutsky BI, Gregor RJ (2000) Analysis of muscle coordination strategies in cycling. IEEE Trans Rehabil Eng 8:362–370

Prilutsky BI, Zatsiorsky VM (2002) Optimization-based models of muscle coordination. Exerc Sport Sci Rev 30:32–38

Prilutsky BI, Gregor RJ, Ryan MM (1998a) Coordination of two-joint rectus femoris and hamstrings during the swing phase of human walking and running. Exp Brain Res 120:479–486

Prilutsky BI, Isaka T, Albrecht AM, Gregor RJ (1998b) Is coordination of two-joint leg muscles during load lifting consistent with the strategy of minimum fatigue? J Biomech 31:1025–1034

Rybak IA, Paton JF, Schwaber JS (1997) Modeling neural mechanisms for genesis of respiratory rhythm and pattern. II. Network models of the central respiratory pattern generator. J Neurophysiol 77:2007–2026

Rybak IA, Ptak K, Shevtsova NA, McCrimmon DR (2003) Sodium currents in neurons from the rostroventrolateral medulla of the rat. J Neurophysiol 90:1635–1642

Rybak IA, Shevtsova NA, Lafreniere-Roula M, McCrea DA (2006a) Modelling spinal circuitry involved in locomotor pattern generation: insights from deletions during fictive locomotion. J Physiol 577:617–639

Rybak IA, Stecina K, Shevtsova NA, McCrea DA (2006b) Modelling spinal circuitry involved in locomotor pattern generation: insights from the effects of afferent stimulation. J Physiol 577:641–658

Safronov BV, Vogel W (1995) Single voltage-activated Na+ and K+ channels in the somata of rat motoneurones. J Physiol 487(Pt 1):91–106

Shevtsova NA (2015) Two-level model of mammalian locomotor CPG. In: Jaeger D, Jung R (eds) Encyclopedia of Computational Neuroscience. New York, NY, Springer, pp. 2999–3017

Shevtsova NA, Chakrabarty S, Hamade K, Markin SN, McCrea DA, Rybak IA (2007) Computational model of mammalian locomotor CPG reproducing firing patterns of flexor, extensor and bifunctional motoneurons during fictive locomotion. In 2014 Neuroscience Meeting Planner. Society for Neuroscience. Abstract 925.4. Washington, DC.

Smith JL, Carlson-Kuhta P, Trank TV (1998a) Forms of forward quadrupedal locomotion. III. A comparison of posture, hindlimb kinematics, and motor patterns for downslope and level walking. J Neurophysiol 79:1702–1716

Smith JL, Carlson-Kuhta P, Trank TV (1998b) Motor patterns for different forms of walking: cues for the locomotor central pattern generator. Ann NY Acad Sci 860:452–455

Stein PSG, Smith JL (1997) Neural and biomechanical control strategies for different forms of vertebrate hindlimb motor tasks. In: Stein P, Grillner S, Selverston AI, Stuart DG (eds) Neurons, networks, and motor behavior. MIT Press, Cambridge, pp 61–73

Stuart DG, Hultborn H (2008) Thomas Graham Brown (1882–1965), Anders Lundberg (1920-), and the neural control of stepping. Brain Res Rev 59:74–95

Wells R, Evans N (1987) Functions and recruitment patterns of one-joint and 2-joint muscles under isometric and walking conditions. Hum Mov Sci 6:349–372